Heavy ion collisions from $\sqrt{s_{NN}}$ of 62.4 GeV down to 7.7 GeV in the EPOS4 framework

K. Werner,[1] J. Jahan,[2] I. Karpenko,[3] T. Pierog,[4] M. Stefaniak,[5,6] and D. Vintache[1]
[1]*SUBATECH, Nantes University–IN2P3/CNRS–IMT Atlantique, 44300 Nantes, France*
[2]*Department of Physics, University of Houston, Houston, Texas 77204, USA*
[3]*Faculty of Nuclear Sciences and Physical Engineering, Czech Technical University in Prague, Břehová 7, Prague, Czech Republic*
[4]*Institute for Astroparticle Physics, Karlsruhe Institute of Technology, Karlsruhe, Germany*
[5]*Department of Physics, The Ohio State University, Columbus, Ohio 43210, USA*
[6]*GSI Helmholtz Centre for Heavy Ion Research, 64291 Darmstadt, Germany*

(Received 5 February 2024; revised 25 October 2024; accepted 13 November 2024; published 6 January 2025)

The EPOS4 project is an attempt to construct a realistic model for describing relativistic collisions of different systems, from proton-proton (pp) to nucleus-nucleus (AA), at energies from several TeV per nucleon down to several GeV. We argue that a parallel scattering formalism (as in EPOS4) is relevant for primary scatterings in AA collisions above 4 GeV, whereas sequential scattering (cascade) is appropriate below. We present briefly the basic elements of EPOS4, and then investigate heavy ion collisions from 62.4 GeV down to 7.7 GeV, to understand how physics changes with energy, studying in particular the disappearance of the fluid component at low energies.

DOI: 10.1103/PhysRevC.111.014903

I. INTRODUCTION

Scatterings of two nuclei are fundamentally different at high energies (several TeV per nucleon) compared to low energies (several GeV). At high energies, one can clearly separate "primary scatterings" happening instantaneously (at $t = 0$) and "secondary scatterings" of the primary particles (for $t > 0$), which may lead to thermalized matter [quark gluon plasma (QGP)] and hadronic rescattering after hadronization. At low energies, one cannot separate these two stages anymore, and at very low energies (<4 GeV), heavy ion collisions can be treated by purely sequential hadronic scatterings, also referred to as hadronic cascade [1–8]. So the physics picture changes drastically when going from several TeV down to a few GeV, and we try to understand these changes. We will start at high energies and we will see how (and when) the "high-energy features" disappear when lowering the collision energies.

Most important for the discussion of primary scatterings at very high energies (several TeV per nucleon) is the observation that nucleon-nucleon scatterings must happen in parallel, and not sequentially, based on very elementary considerations concerning timescales. To take this "parallel scattering scenario" into account, EPOS4 brings together ancient knowledge about S-matrix theory (to deal with parallel scatterings) and modern concepts of perturbative QCD and saturation, going much beyond the usual factorization approach; see Refs. [9–12].

Let us look more in detail at the relevant timescales (see Ref. [11] for details). The particle (hadron) formation time $\tau_{\rm form}$ has to be compared to the collision time $\tau_{\rm collision}$ (the duration of an AA collision) and to the interaction time $\tau_{\rm interaction}$ (time between two nucleon-nucleon interactions). We define the high-energy threshold $E_{\rm HE}$ (in the sense of energy $\sqrt{s_{NN}}$ per nucleon-nucleon pair) by the identity

$$\tau_{\rm form} = \tau_{\rm collision}, \tag{1}$$

and the low-energy threshold $E_{\rm LE}$ by the identity

$$\tau_{\rm form} = \tau_{\rm interaction}. \tag{2}$$

Considering central rapidity hadrons ($\gamma_{\rm hadron} = 1$), a formation time $\tau_{\rm form} = 1\,{\rm fm}/c$, and a big nucleus with $R = 6.5\,{\rm fm}$, we get [11]

$$E_{\rm LE} \approx 4\,{\rm GeV}, \quad E_{\rm HE} \approx 24\,{\rm GeV}. \tag{3}$$

Beyond $E_{\rm HE}$ particle production starts only after the two nuclei have passed through each other, which means all the nucleon-nucleon collisions should happen in parallel, instantaneously, there is no time sequence. Below $E_{\rm LE}$ a hadronic cascade is appropriate. Between the two thresholds, one needs some "partially parallel scattering scenario," which is not yet implemented in EPOS4. We will employ the full "parallel scattering scenario" down to lowest energies, and we will investigate where precisely and how it breaks down. Since PbPb at 5.02 ATeV and AuAu at 200 GeV have already been discussed in Ref. [11], we will focus in this paper on energies below 200 GeV.

In the overview in Ref. [9] and in detail in Refs. [10,11] it is shown how such a "parallel scattering scheme" for

primary scatterings can be constructed, based on S-matrix theory, which we will sketch very briefly in the following.

An early realization is the Gribov-Regge (GR) approach [13–16] for pp and AA scatterings. This S-matrix approach has a modular structure, it is based on so-called "cut Pomerons," representing elementary parton-parton scatterings, with the associated mathematical object $G = \mathrm{cut}T$, with T being the Fourier transform (with respect to the momentum transfer) of the corresponding T-matrix, divided by $2s$, with s referring to the Mandelstam variable. This so-called "impact parameter representation" with $G = G(b)$ with an impact parameter b makes formulas simpler. Although the GR approach is an excellent tool to deal with parallel scatterings, a serious drawback is the fact that the energy-momentum sharing between the multiple scatterings is not taken care of. And obviously GR has no answer to the question of how to connect the cut Pomeron expression G and the corresponding QCD expression G_{QCD} for parton-parton scattering.

In Ref. [17], a possible solution has been proposed, by taking into account energy-momentum sharing (let us call this approach "GR$^+$") and based on the hypothesis "G is equal to G_{QCD}," where the latter is essentially a cut parton ladder based on DGLAP parton evolutions [15,18,19]. A detailed discussion about the calculation of G_{QCD} can be found in Ref. [10]. Unfortunately, it turned out that implementing energy-momentum sharing has a very negative side effect: it ruins seriously elementary geometric properties such as binary scaling in AA scattering. In EPOS4, the first step toward a solution of the problem is a detailed understanding of what causes the problem and that it is fundamental, and not just a wrong parameter choice. Using

$$G = G_{\mathrm{QCD}} \tag{4}$$

leads unavoidably to contradictions. In a second step, a solution could be presented. Let us look at the arguments of G and G_{QCD}: Both depend on b (not written explicitly) and on the lightcone momenta of the external legs x^+ and x^-. But most importantly, G_{QCD} also depends on some low virtuality cutoff fo the parton evolution, and this cutoff is now considered to not anymore be simply a constant, but a dynamical variable, named saturation scale Q^2_{sat}. So we have $G_{\mathrm{QCD}} = G_{\mathrm{QCD}}(Q^2_{\mathrm{sat}}, x^+x^-)$. The fundamental relation between G and G_{QCD} is now

$$G(x^+, x^-) = \frac{n}{R_{\mathrm{deform}}(N_{\mathrm{conn}}, x^+, x^-)} G_{\mathrm{QCD}}\big(Q^2_{\mathrm{sat}}, x^+, x^-\big), \tag{5}$$

with $Q^2_{\mathrm{sat}} = Q^2_{\mathrm{sat}}(N_{\mathrm{conn}}, x^+, x^-)$ and with (being crucial)

$$G \text{ independent of } N_{\mathrm{conn}}, \tag{6}$$

with the so-called connection number N_{conn} counting the number of Pomerons being connected to the same projectile and target nucleon as the given Pomeron. The quantity $R^{(N_{\mathrm{conn}})}_{\mathrm{deform}}$ is the deformation of the distribution of x^+x^- (the Pomeron's energy squared) in the case of $N_{\mathrm{conn}} > 1$ compared to the case $N_{\mathrm{conn}} = 1$. This deformation (a consequence of several Pomerons competing for energy sharing) destroys factorization and binary scaling unless one uses Eqs. (5) and (6). Finally, n is a normalization constant.

TABLE I. Energy-dependent parameters.

Energy	$P1$	$P2$	$P3$	$P4$
4.0	1.0	2.0	1.0	2.0
7.7	1.7	2.0	1.0	2.0
11.5	2.0	3.8	1.0	1.5
14.0	2.0	4.2	1.0	1.5
19.6	3.0	4.7	1.0	1.5
27.0	3.0	5.0	1.0	1.5
39.0	3.0	5.0	1.0	1.5
62.4	5.5	5.5	1.0	1.0

The primary scattering will produce "parton-ladders." The link between primary and secondary scatterings is the "core-corona procedure": The parton ladders are treated as classical relativistic (kinky) strings. So in general, we have a large number of (partly overlapping) strings. Based on the momenta and the density of string segments (referred to as prehadrons in the following), one separates at some early proper time τ_0 the core (going to be treated as fluid) from the corona (escaping hadrons, including jet hadrons).

We will first discuss, in Sec. II, particle production and the role of core, corona, and remnants for different energies, down to 4 GeV.

Then in Secs. III, IV, V, and VI, we will show very detailed results from 62.4 GeV down to 7.7 GeV, considering the transverse momentum dependencies of yields and flow harmonics v_2

(i) for all energies,
(ii) for all possible centrality choices, and
(iii) for all hadron species where the corresponding data exist, namely pions, kaons, (anti)protons, but also hyperons (Λ, Ξ, Ω) and Φ mesons.

This is the most complete collection of model/data comparisons concerning gold-gold collisions in this energy domain, in particular concerning differential yields (p_t dependencies).

Certain model parameters need to be energy dependent, deduced from comparisons with experimental data, and for the moment they are given in terms of a table. In the EPOS4 framework, remnants play an important role, their mass distribution is assumed to be given according to a law $(m^2)^{-2.5}$ for $m > P1 + Z * (P2 - P1)$. In EPOS, $t = 0$ is defined as the time corresponding to maximal overlap of the colliding nuclei. Fluidization takes place at a fixed proper time $\tau = \tau_0$, which we later call initial proper time. It is assumed to be $P3 + Z * (P4 - P3)$, with the parameters as given in Table I and wit Z representing the centrality in terms of $N_{\mathrm{part}}/N^{\mathrm{max}}_{\mathrm{part}}$.

In the EPOS4 framework, the start time τ_0 affects final results only moderately, earlier times make the p_t distributons a bit harder. The current parameters $P3$ and $P4$ have been chosen to optimize the pt spectra. However, the mass distributions of the remnants are crucial for particle production at large rapidities.

Over the past decade, a few other models involving a fluid dynamic picture have been developed for the energy range $\sqrt{s_{\rm NN}} = 7.7$–62.4 GeV, where the UrQMD cascade [20], a decelerating string picture [21,22], and a 3D extension to Monte Carlo Glauber [23] have been employed for the initial state. These models succeeded in reproducing the collision energy dependence of the shape and the magnitude of the rapidity density of hadrons, and (except Refs. [21,22]) of p_t-integrated yields and elliptic flow coefficients. In Ref. [20], transverse momentum spectra of several hadron species at selected centralities and energies were shown.

II. ROLE OF CORE, CORONA, AND REMNANTS FOR DIFFERENT ENERGIES

Multiple scattering diagrams (representing the primary scatterings) are the origin of particle production, which means first the production of so-called prehadrons, having the quantum numbers of hadrons, but not necessarily being final. Prehadrons originate from Pomerons (via kinky strings) or from remnants. A detailed description can be found in Sec. 4 of Ref. [10], where we also discuss the different types of Pomerons and their relation with pQCD, including technical details for the pQCD computations.

The pQCD part (parton ladders) is a crucial element of a Pomeron at LHC energies. But with decreasing energy, it becomes more and more likely that these Pomerons are replaced by purely soft ones, see Sec. 3 of Ref. [12]. At 200 GeV, the relative weight of "normal" compared to soft Pomerons is roughly 1:1, at even lower energies, the soft dominates. Also the Pomerons get less energetic, producing fewer particles.

Based on these abovementioned prehadrons, we employ a so-called core-corona procedure (see Ref. [24], for a more recent discussion in the EPOS4 framework see Ref. [12]), to distinguish core from corona particles, at some given (early) proper-time τ_0. The core prehadrons constitute "bulk matter" and will be treated via hydrodynamics. The corona prehadrons become simply hadrons and propagate with reduced energy (due to some energy loss). Corona particles are either very energetic (then they move out even from the center), or they are close to the surface, or we have a combination of both.

We will try to understand the relative importance of the core part and of the fraction coming from remnant decay. In Fig. 1, we show results for central (0–5%) PbPb collisions at 5.02 TeV, and central (0–5%) AuAu collisions from 200 down to 4 GeV (per nucleon). We plot four different curves: all prehadrons (red full), all core prehadrons (red dotted), prehadrons from remnant decay (blue thin full), and core prehadrons from remnant decay (blue thin dashed). Looking at the results for PbPb at 5.02 TeV, we observe that almost all prehadrons are core prehadrons, so the core dominates. Prehadrons from remnants are preferentially produced at large rapidities, but also here almost all are core prehadrons. Going down in energy, starting already at 200 GeV, we see that the core still dominates around $\eta = 0$, but at large values of $|\eta|$, the core contribution drops dramatically. We also observe that the remnant contributions become more and more important, and very dominant below 20 GeV. Nevertheless, close to $\eta = 0$, the core remains dominant—down to 7.7 GeV. There

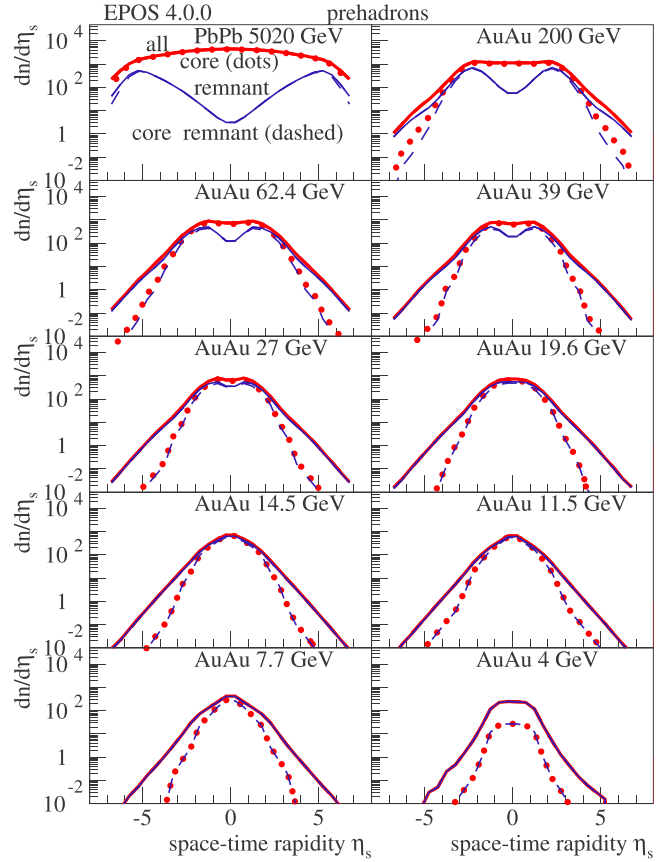

FIG. 1. The prehadron yield as a function of space-time rapidity [$\eta_s = \frac{1}{2}\ln((t+z)/(t-z))$, with t being the time and z the longitudinal coordinate], for central AA collisions at different energies. The curves refer to all prehadrons (red full), all core prehadrons (red dotted), prehadrons from remnant decay (blue thin full), and core prehadrons from remnant decay (blue thin dashed).

is actually little change from 39 down to 7.7 GeV, but things change from 7.7 to 4 GeV: the core part decreases strongly.

Based on core pre-hadrons, we compute the corresponding energy-momentum tensor $T^{\mu\nu}$ and the flavor flow vector at some position x at initial proper time $\tau = \tau_0$ as

$$T^{\mu\nu}(x) = \sum_i \frac{p_i^\mu p_i^\nu}{p_i^0} g(x - x_i) \tag{7}$$

and

$$N_q^\mu(x) = \sum_i \frac{p_i^\mu}{p_i^0} q_i\, g(x - x_i), \tag{8}$$

with $q_i \in u, d, s$ being the net flavor content and p_i the four-momentum of prehadron i. The function g is some Gaussian smoothing kernel (see Ref. [12]). The Lorentz transformation into the comoving frame provides the energy density ε and the flow velocity components v^i, which will be used as the initial condition for a hydrodynamical evolution [25]. This is based on the hypothesis that equilibration happens rapidly and affects essentially the space components of the energy-momentum tensor. In Fig. 2, we plot the energy density and the baryon density at the initial proper-time τ_0 as a function

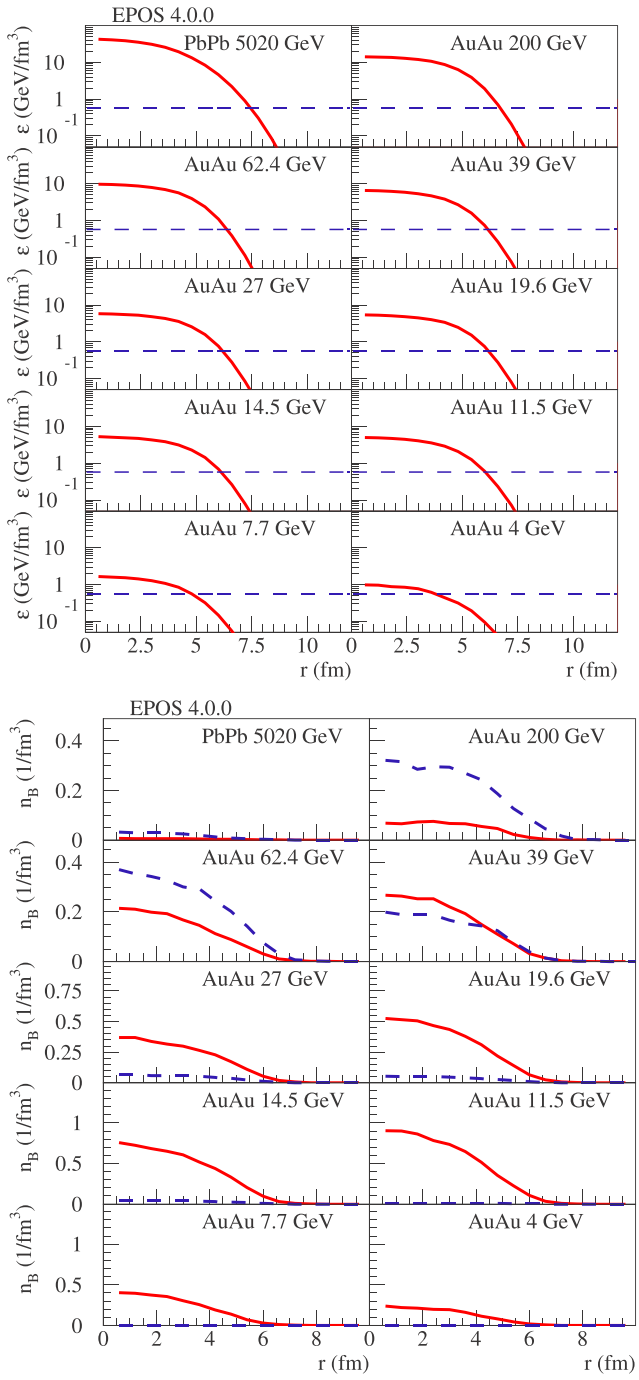

FIG. 2. Energy density (upper plot) and baryon density (lower plot) at the initial proper-time τ_0 as a function of the transverse coordinate r for central AA collisions at different energies. The horizontal blue dashed line is the freeze-out energy density. The red solid lines refer to $\eta_s = 0$ and the blue dashed lines to $\eta_s = 2$.

of the transverse coordinate r in AA collisions at different energies.

Concerning the energy density, in Fig. 2 (upper plot), we also indicate as a blue dashed line the freeze-out energy density $\varepsilon_{\rm FO}$. At the highest energies, the energy density is way above the critical value $\varepsilon_{\rm FO}$, but with decreasing beam energy, the energy density approaches this value. At 4 GeV, the energy density is just slightly above $\varepsilon_{\rm FO}$. Going to lower energies, the baryon densities even at central rapidities become an issue. In Fig. 2 (lower plot), we plot the baryon density at the initial proper-time τ_0 as a function of the transverse coordinate r in AA collisions at different energies. for space-time rapidity $\eta_s = 0$ and $\eta_s = 2$. In the case of PbPb collisions at 5.02 TeV, the baryon number is small, for both $\eta_s = 2$ choices. Considering AuAu collisions at 200 GeV, we observe a baryon density of around $0.3\,\mathrm{GeV/fm^3}$ at $\eta_s = 2$, but a much smaller value at $\eta_s = 0$. Decreasing the energy, we observe a more and more increasing baryon density density, becoming bigger than the value at $\eta_s = 2$. Below 20 GeV, we get baryon densities bigger than $0.5\,\mathrm{GeV/fm^3}$ at $\eta_s = 0$, but more than ten times smaller at $\eta_s = 0$. At 7.7 and 4 GeV, the baryon density decreases compared to 11.5 GeV, due to a bigger corona part (energy density and baryon density refer of course to the core). In the first version of this paper, there was no core created at 4 GeV due to a requirement for the core to have at least one prehadron from Pomerons contributing (and not only remnant contributions). This requirement has no effect at energies beyond 7.7 GeV, but it has an effect at very low energies. Dropping that condition (commenting one line in the code), we do get a core at 4 GeV with an energy density slightly above $\varepsilon_{\rm FO}$.

As a next step, the core part of the system evolves according to the equations of relativistic viscous hydrodynamics [25,26], where we use presently $\eta/s = 0.08$. The "core-matter" hadronizes on some hyper-surface defined by a constant energy density $\epsilon_{\rm FO}$ (presently $0.57\,\mathrm{GeV/fm^3}$). In earlier versions [27], we used a so-called Cooper-Frye procedure. This is problematic in particular for small systems: not only energy and flavor conservation become important, but we also encounter problems due to the fact that we get small "droplets" with huge baryon chemical potential, with strange results for heavy baryons. In EPOS4, we will systematically use microcanonical hadronization, with major technical improvements compared to earlier versions (see Ref. [12]).

In the following, we want to study core and corona contributions to hadron production. We will distinguish:

(A): The "*core + corona*" contribution: primary interactions (S-matrix approach for parallel scatterings), plus core-corona separation, hydrodynamic evolution and microcanonical hadronization of the core, but without hadronic rescattering.

(B): The "*core*" contribution: as (A), but considering only core particles.

(C): The "*corona*" contribution: as (A), but considering only corona particles.

(D): The "*full*" EPOS4 scheme: as (A), but in addition hadronic rescattering.

In cases (A), (B), and (C), we need to exclude the hadronic afterburner, because the latter affects both core and corona particles, so in the full approach, the core and corona contributions are not visible anymore. In the following, we will focus on energies below 200 GeV, since the corresponding plots for PbPb at 5.02 ATeV and AuAu at 200 GeV have already been discussed in Ref. [11].

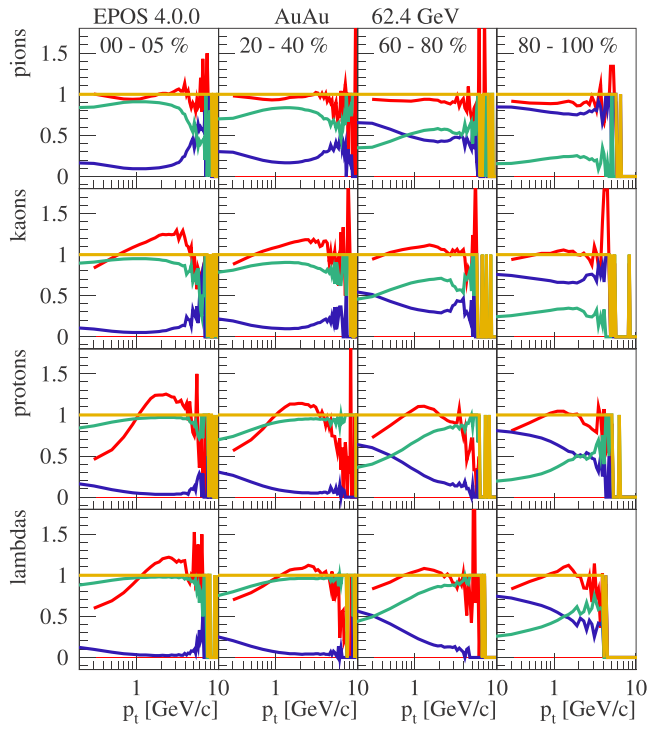

FIG. 3. The X/core + coron ratio, with X being the corona contribution (blue), the core (green), and the full contribution (red), for four centrality classes and four different particle species, for AuAu at 62.4 GeV.

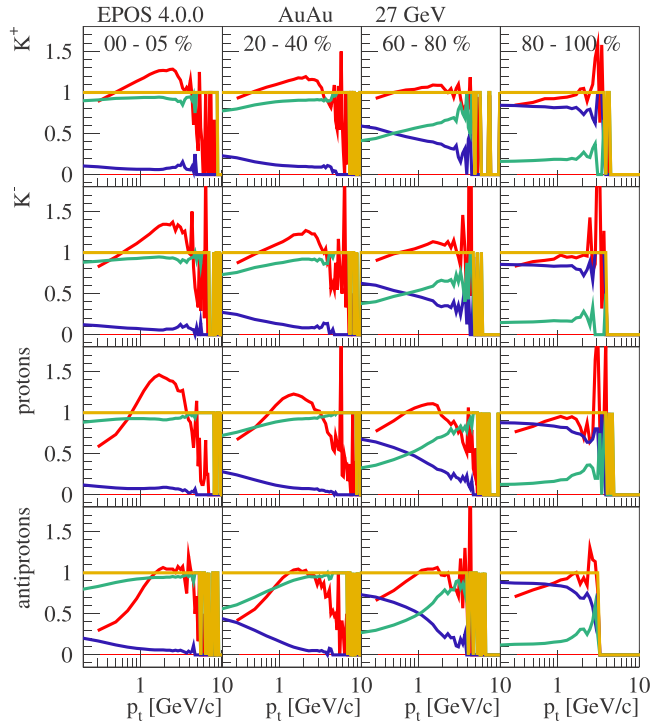

FIG. 5. Same as Fig. 4, but for 27 GeV.

In Figs. 3–6, we show ratios X/core + corona versus p_t, with X being the corona contribution (blue), the core (green), and the full contribution (red), for AuAu collisions at different energies. In Fig. 3, we show results at 62.4 GeV, for (from top to bottom) pions ($\pi^{\pm}$), kaons ($K^{\pm}$), protons (p and $\bar{p}$),

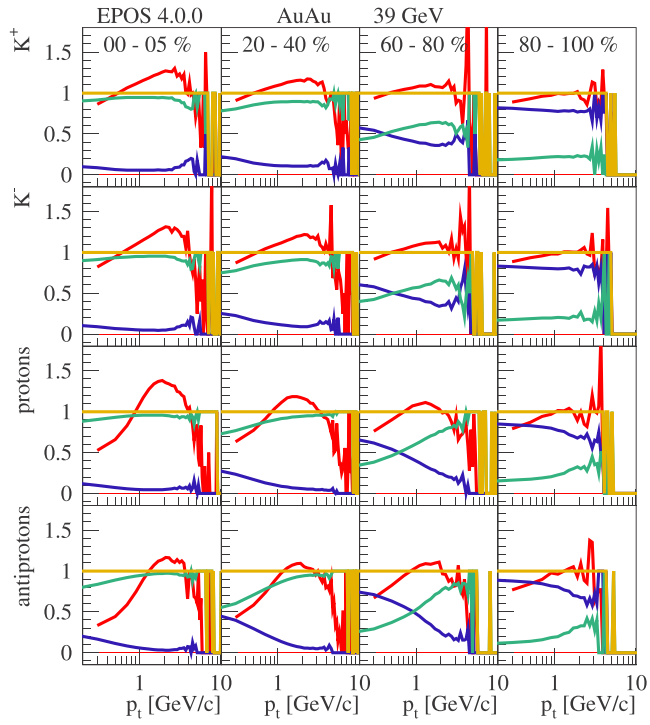

FIG. 4. Same as Fig. 3, but for 39 GeV, and we consider K^+, K^-, p, and $\bar{p}$ hadrons.

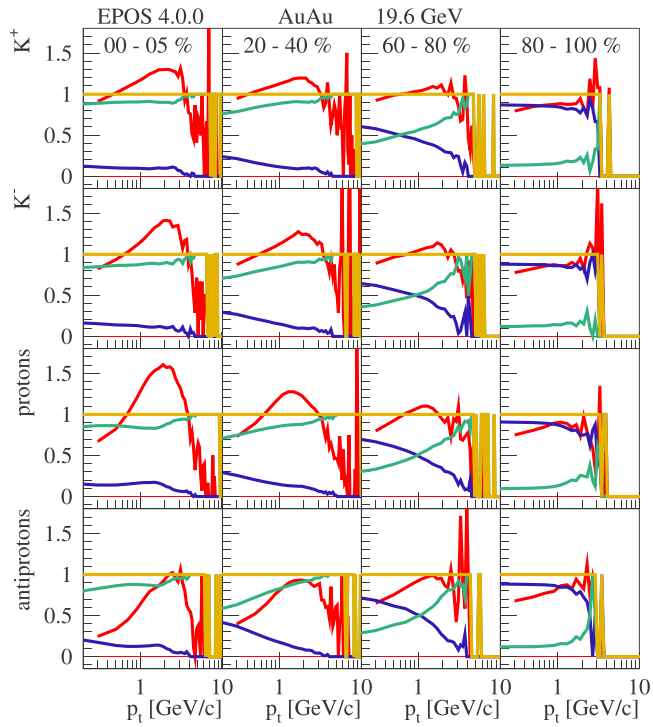

FIG. 6. Same as Fig. 4, but for 19.6 GeV.

and lambdas (Λ and $\bar{\Lambda}$). The four columns represent four different centrality classes, namely, 0–5%, 20–40%, 60–80%, and 80–100%. Looking at the green (core) and blue (corona) curves, we observe that the core contribution increases from peripheral to central collisions. We observe a maximum of the green core curves around $1-2$ GeV/c, at very low p_t the core contribution goes down, so even at very small p_t values the corona contributes. At higher energies (see Ref. [11]), one observes a crossing of the green core and the blue corona curves (core exceeds corona toward high p_t) between around 2 GeV/c (mesons, peripheral) and 5 GeV/c (baryons, central), and for larger values the corona contribution dominates clearly. Here, the crossing is absent (except for pions for 0–5% at 62.4 GeV). There are two reasons. The spectra are softer compared to higher energies, and around 3–6 GeV/c, the core and corona curves are almost parallel. And since high p_t becomes rare, we cannot reach very high p_t in the Monte Carlo simulations.

The red curve, full over core + corona, represents the effect of the hadronic cascade in the full case. The pions are not much affected, but for kaons and even more for protons and lambdas, rescattering makes the spectra harder. We should keep in mind that rescattering involves particles from fluid hadronization, but also corona particles from hard processes. Concerning the baryons, rescattering reduces (considerably) low p_t yields, due to baryon-antibaryon annihilation. In Figs. 4–6, we show results for AuAu collisions at 39, 27, and 19.6 GeV. The high p_t particles are getting rare, we hardly get (for simulations with reasonable CPU times) beyond 5 GeV/c. Another "low energy effect": the difference between particles and antiparticles becomes more and more important, this is why we consider separately K^+, K^-, p, and $\bar{p}$. The biggest effect can be seen when comparing the effect of hadronic rescattering (red curves) for protons and antiprotons: with decreasing energy, the proton curve goes slightly up, and the antiproton curve goes significantly down (they are rare, and most of them are annihilated). Interesting observation: also at lower energies, the core ratios (green curves) get down at low p_t, but stay close to unity at intermediate p_t.

Corresponding plots for AuAu collisions at 11.5 and 7.7 GeV can be found in the Appendix.

When discussing these results at low energies (7.7–19.6 GeV), we should keep in mind our discussion in Sec. I, where we estimated that our parallel scattering scenario should be valid beyond 24 GeV per nucleon, and below we have to take into account the fact that particle production starts before the two nuclei have passed through each other (not yet done in EPOS4).

But anyway, in the following sections, we will explore to what extent the model "works" (and can explain data), and where it fails, and what we can learn from that.

III. RESULTS CONCERNING P_T SPECTRA

In this section, we show simulation results compared to data. We will not add too many comments to each curve, the main purpose is to check if the concepts discussed in the previous sections give a coherent picture (and reproduce the data) or not.

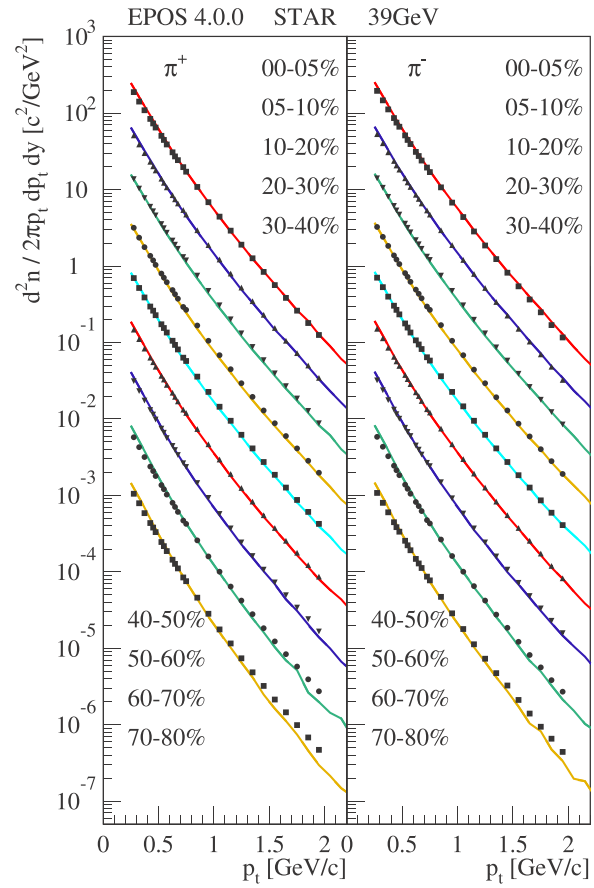

FIG. 7. Transverse momentum distributions of π^+, π^- in AuAu collisions at 39 GeV for different centrality classes. EPOS4 simulation (lines) are compared to data from STAR [28]. From top to bottom, we multiply the curves by 3^{-i}, $i = 0, 1, 2, 3, \ldots$.

The number of plots is huge, and it would be tempting to show only a selection of results and provide a simple message. And it would be tempting to optimize parameters to have "nice" plots. But the EPOS4 philosophy is different: It is an attempt to have a single unique approach, with version number (here 4.0.0), and make a maximum of tests, as complete as possible, for all kinds of observables and at various energies. Modeling heavy ion collisions is complex, consisting of several stages, with considerable uncertainties at each step. And there is nothing like the simple "smoking gun" to prove or disprove certain concepts. Flow harmonics, for example, are popular observables showing the effect of flow asymmetries, but the flow affects also the p_t spectra, more or less strongly depending on the mass of the particle. So rather than looking at few selected curves and expecting precision results, the idea is here more to get a global view and to see to what extent a given theoretical scenario can provide an overall good description of a very large set of data.

We will see later, that p_t spectra and elliptical flow v_2, although both are affected by flow, they are at a different degree sensitive to particular details of the model, so we get complementary information, and therefore both observables should be studied.

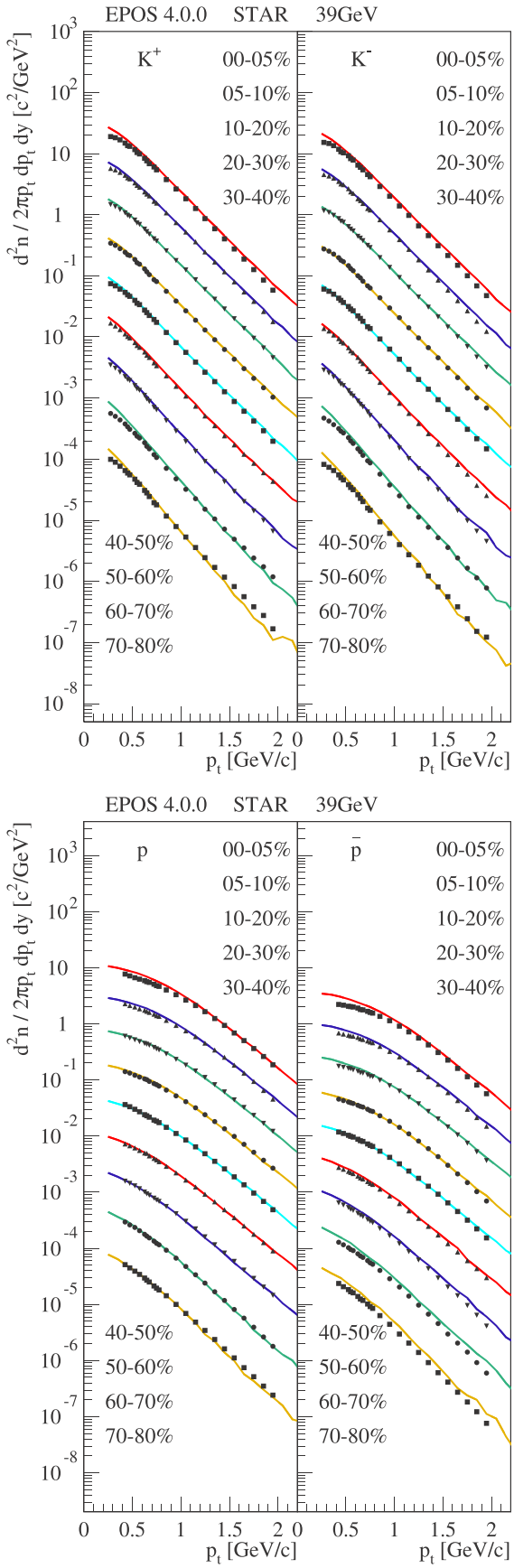

FIG. 8. Same as Fig. 7, but for K^+, K^-, p, $\bar{p}$.

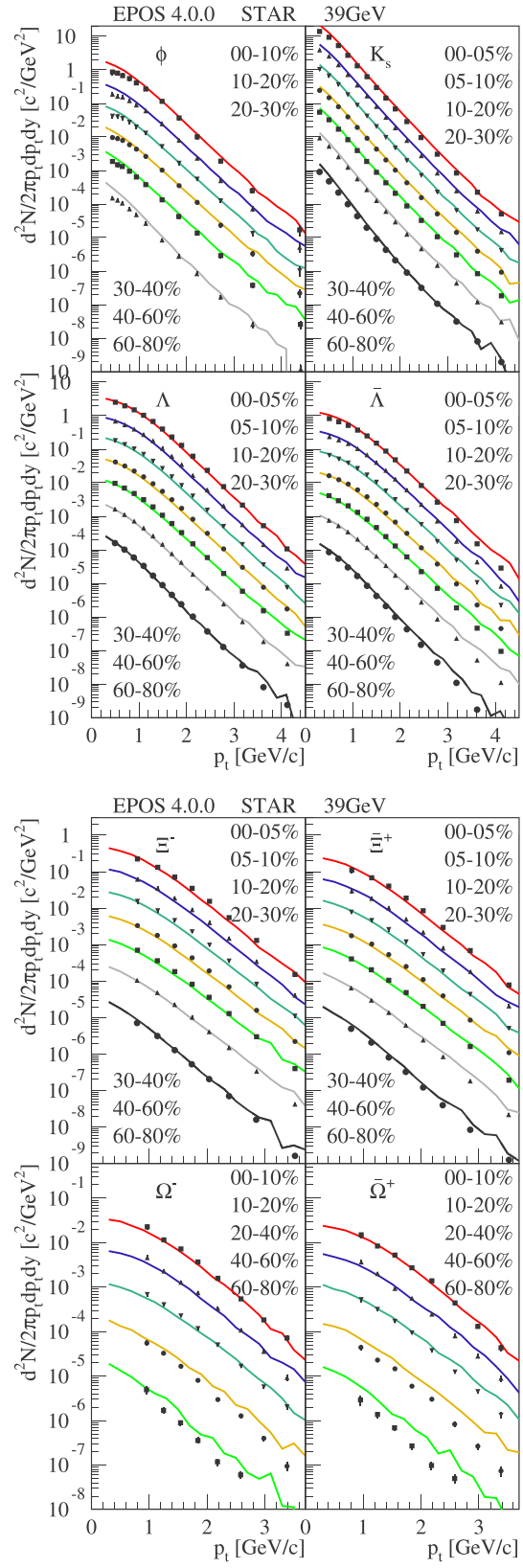

FIG. 9. Transverse momentum distributions of ϕ, K_0, Λ, $\bar{\Lambda}$ Ξ^-, $\bar{\Xi}^+$, Ω^-, $\bar{\Omega}^+$ in AuAu collisions at 39 GeV at central rapidity for different centralities. EPOS4 simulation (lines) are compared to data from STAR [29].

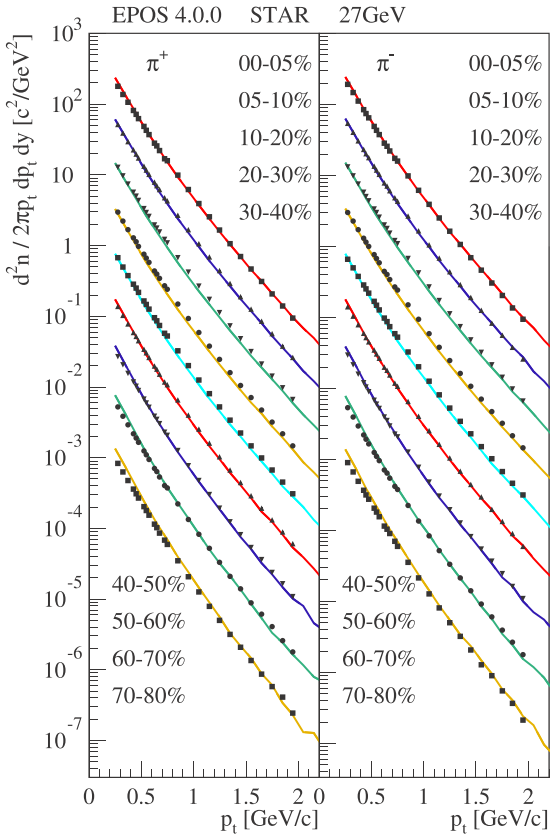

FIG. 10. Transverse momentum distributions of π^+, π^- in AuAu collisions at 27 GeV for different centrality classes. EPOS4 simulation (lines) are compared to data from STAR [28]. From top to bottom, we multiply the curves by 3^{-i}, $i = 0, 1, 2, 3, \ldots$.

This "global view" strategy requires a huge amount of tests, and therefore the "tuning" of parameters and options is far from being optimized, But we expect reasonable agreement in the energy range (beyond 24 GeV) where the parallel scattering approach is applicable.

In the following we discuss p_t spectra. We will start with the highest energy, and then move down till 7.7 GeV per nucleon. To go this way is convenient in the sense that from the theory point of view, in our model, the high-energy case contains in principle everything, we do not need to add "features" at low energies, simply certain phenomena "die out," like the hard Pomerons which dominate particle production at the LHC. For more details see Ref. [12].

We will focus on energies from 39 GeV down to 7.7 GeV, the corresponding plots for PbPb at 5.02 TeV and AuAu at 200 GeV have already been discussed in Ref. [11].

Some discussion concerning decay channels and weak decay handling can be found in Appendix B.

A. Results for 39 GeV

In Figs. 7 and 8, we show transverse momentum distributions of $\pi^+, \pi^-, K^+, K^-, p, \bar{p}$ in AuAu collisions at 39 GeV for different centrality classes. EPOS4 simulation (lines) are

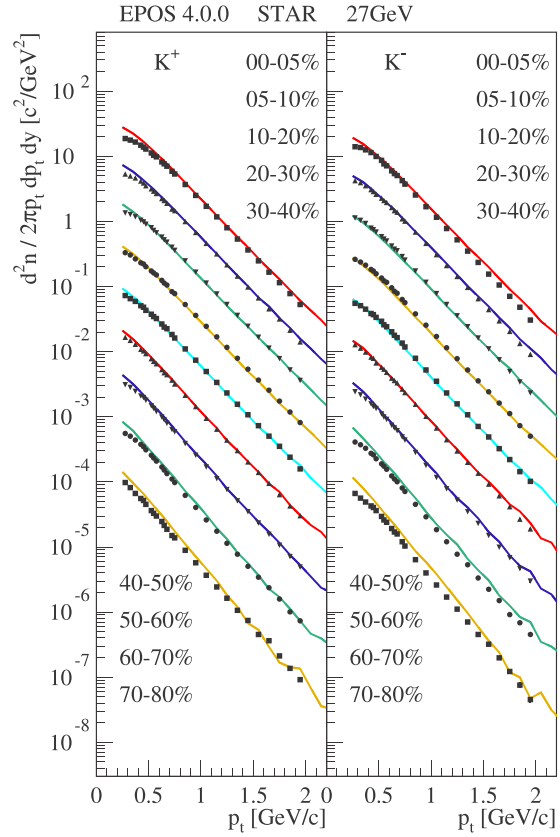

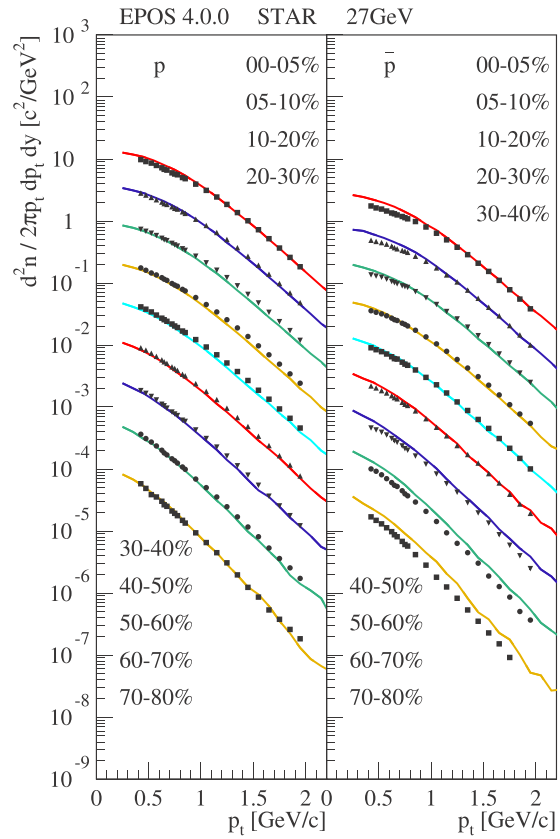

FIG. 11. Same as Fig. 10, but for $K^+, K^-, p, \bar{p}$.

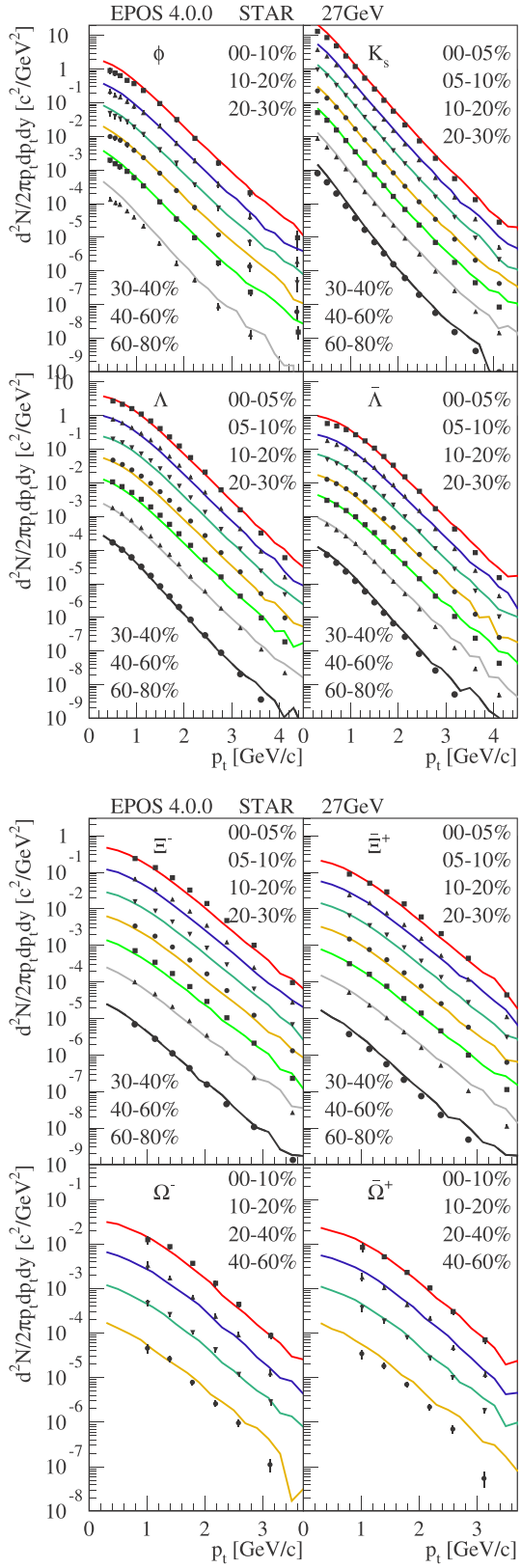

FIG. 12. Transverse momentum distributions of ϕ, K_0, Λ, $\bar{\Lambda}$ Ξ^-, $\bar{\Xi}^+$, Ω^-, $\bar{\Omega}^+$ in AuAu collisions at 27 GeV at central rapidity for different centralities. EPOS4 simulation (lines) are compared to data from STAR [29].

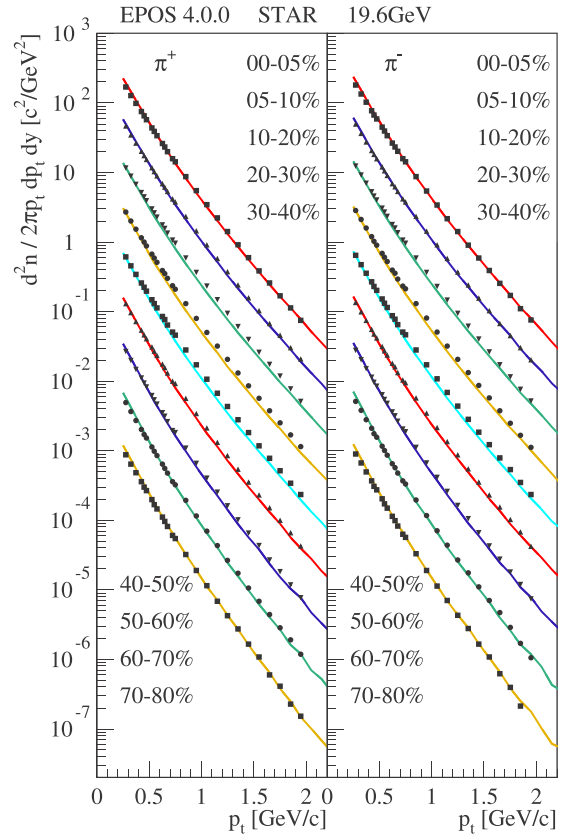

FIG. 13. Transverse momentum distributions of π^+, π^- in AuAu collisions at 19.6 GeV for different centrality classes. EPOS4 simulation (lines) are compared to data from STAR [28]. From top to bottom, we multiply the curves by 3^{-i}, $i = 0, 1, 2, 3, \ldots$.

compared to data from STAR [28]. From top to bottom, we multiply the curves by 3^{-i}, $i = 0, 1, 2, 3, \ldots$.

In Fig. 9, we show transverse momentum distributions of ϕ, K_0, Λ, $\bar{\Lambda}$ Ξ^-, $\bar{\Xi}^+$, Ω^-, $\bar{\Omega}^+$ in AuAu collisions at 39 GeV at central rapidity for different centralities. EPOS4 simulation (lines) are compared to data from STAR [29].

In general, the simulation results are close to the data, concerning identified particles as pions, kaons, and protons, and as well as hyperons, although for kaons and antiprotons at low p_t the simulations are slightly above the data. Concerning the ϕ meson, the simulations are somewhat above the data at low p_t.

B. Results for 27 GeV

In Figs. 10 and 11, we show transverse momentum distributions of π^+, π^-, K^+, K^-, p, $\bar{p}$ in AuAu collisions at 27 GeV for different centrality classes. EPOS4 simulation (lines) are compared to data from STAR [28]. From top to bottom, we multiply the curves by 3^{-i}, $i = 0, 1, 2, 3, \ldots$.

In Fig. 12, we show transverse momentum distributions of ϕ, K_0, Λ, $\bar{\Lambda}$ Ξ^-, $\bar{\Xi}^+$, Ω^-, $\bar{\Omega}^+$ in AuAu collisions at 27 GeV at central rapidity for different centralities. EPOS4 simulation (lines) are compared to data from STAR [29].

In general, the simulation results are relatively close to the data, concerning identified particles as pions, kaons, and

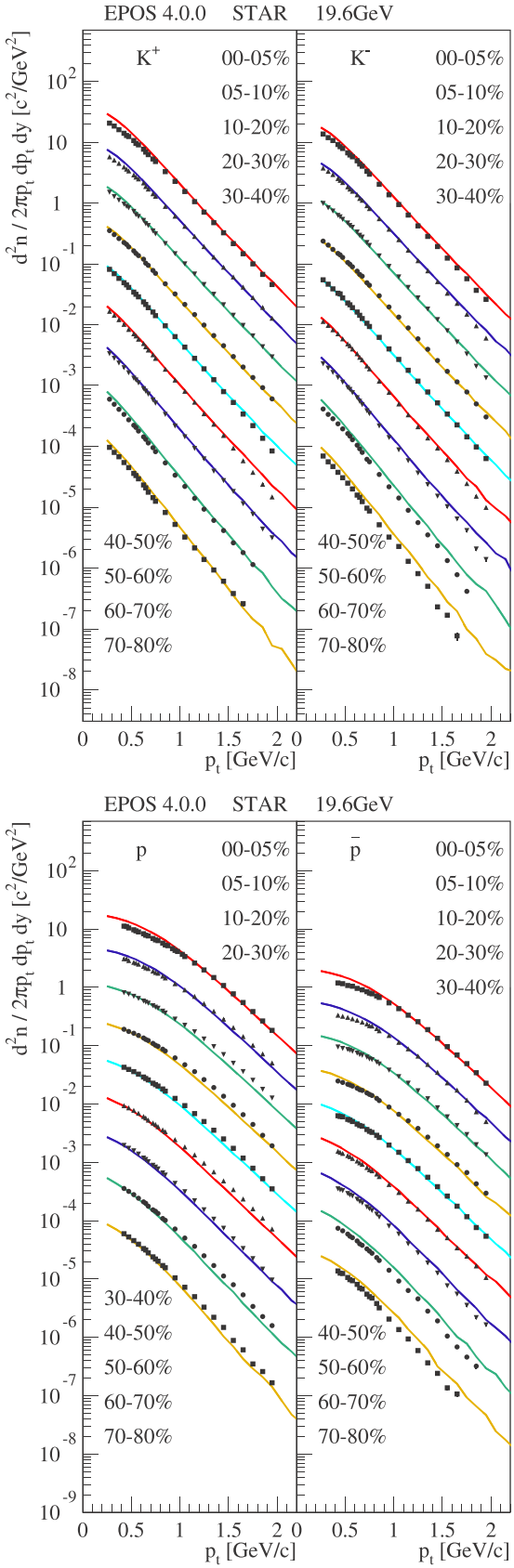

FIG. 14. Same as Fig. 13, but for K^+, K^-, p, $\bar{p}$.

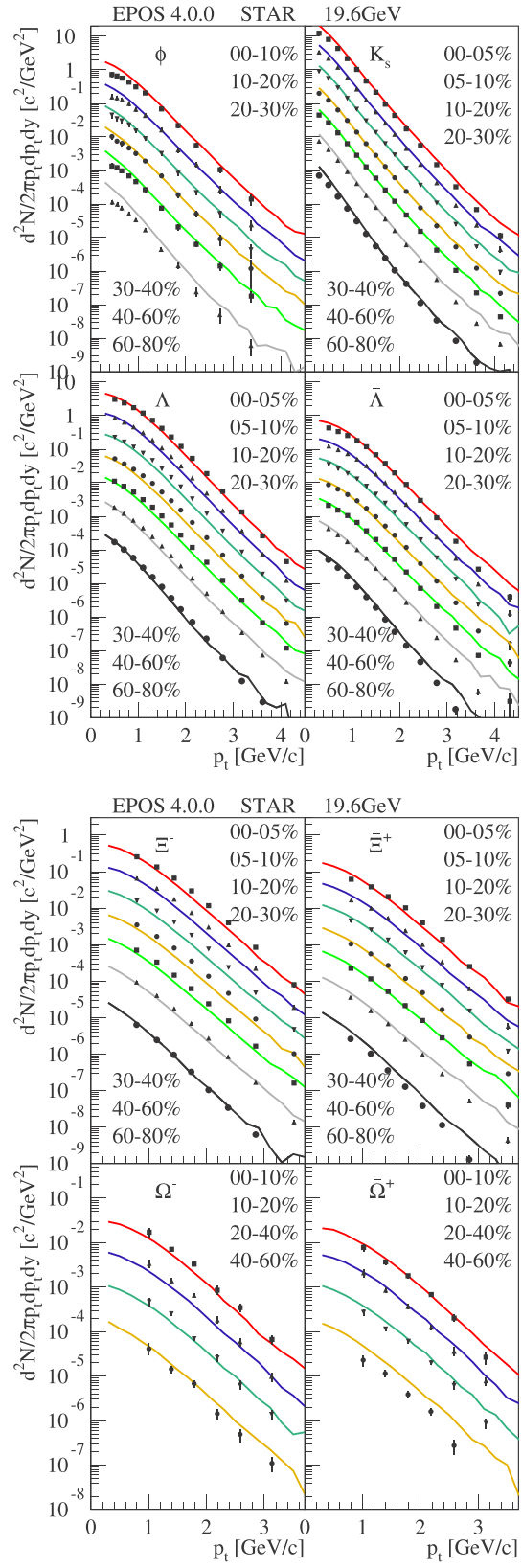

FIG. 15. Transverse momentum distributions of ϕ, K_0, Λ, $\bar{\Lambda}$ Ξ^-, $\bar{\Xi}^+$, Ω^-, $\bar{\Omega}^+$ in AuAu collisions at 19.6 GeV at central rapidity for different centralities. EPOS4 simulation (lines) are compared to data from STAR [29].

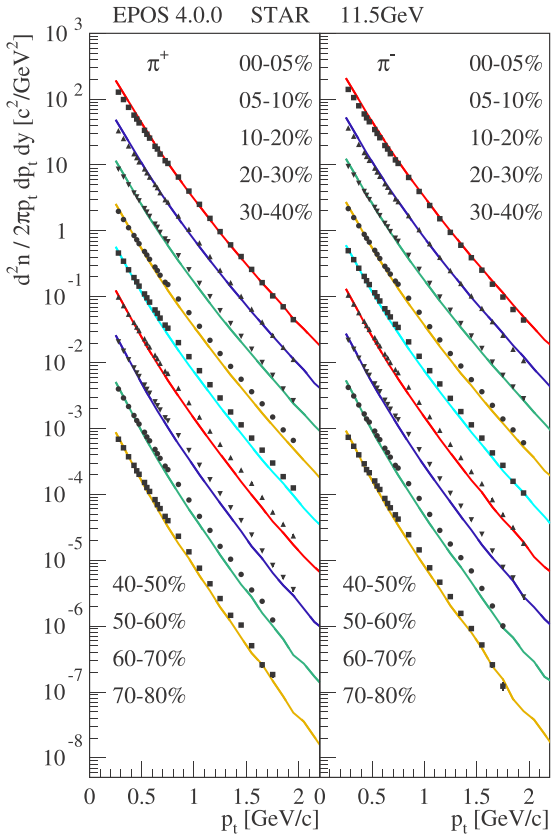

FIG. 16. Transverse momentum distributions of π^+, π^- in AuAu collisions at 11.5 GeV for different centrality classes. EPOS4 simulation (lines) are compared to data from STAR [28]. From top to bottom, we multiply the curves by 3^{-i}, $i = 0, 1, 2, 3, \ldots$.

protons, and as well hyperons. But compared to 39 GeV, for kaons, antiprotons, and the ϕ meson, the deviation (simulation compared to data) at low p_t gets bigger.

C. Results for 19.6 GeV

In Figs. 13 and 14, we show transverse momentum distributions of π^+, π^-, K^+, K^-, p, $\bar{p}$ in AuAu collisions at 19.6 GeV for different centrality classes. EPOS4 simulation (lines) are compared to data from STAR [28]. From top to bottom, we multiply the curves by 3^{-i}, $i = 0, 1, 2, 3, \ldots$.

In Fig. 15, we show transverse momentum distributions of ϕ, K_0, Λ, $\bar{\Lambda}$ Ξ^-, $\bar{\Xi}^+$, Ω^-, $\bar{\Omega}^+$ in AuAu collisions at 19.6 GeV at central rapidity for different centralities. EPOS4 simulation (lines) are compared to data from STAR [29].

In general, the simulation results are relatively close to the data, concerning identified particles as pions, kaons, and protons, and as well hyperons. Similar to what we have already seen at 27 GeV, for kaons, antiprotons, and the ϕ meson, the simulation is somewhat above the data.

D. Results for 11.5 GeV

In Figs. 16 and 17, we show transverse momentum distributions of π^+, π^-, K^+, K^-, p, $\bar{p}$ in AuAu collisions at 11.5 GeV for different centrality classes. EPOS4 simulation (lines)

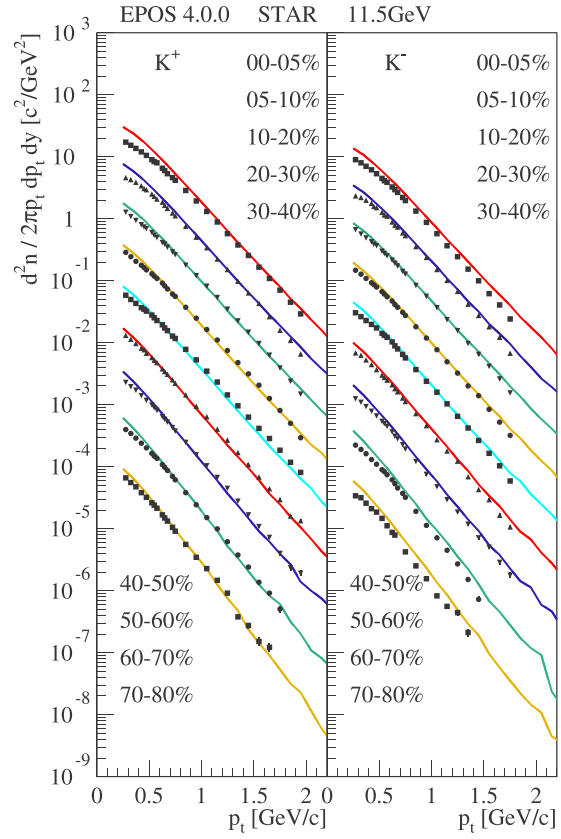

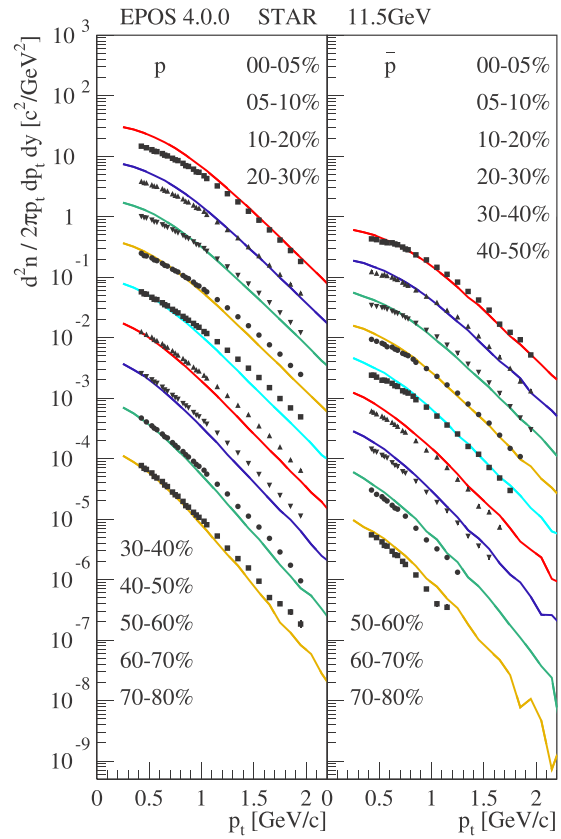

FIG. 17. Same as Fig. 16, but for K^+, K^-, p, $\bar{p}$.

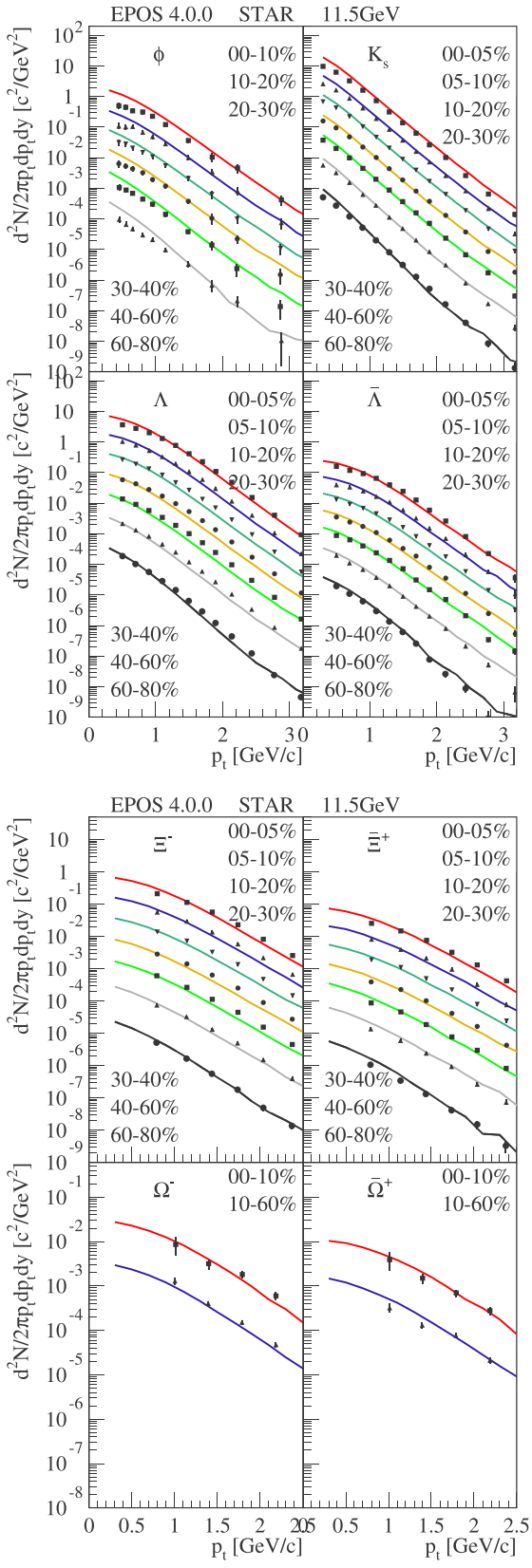

FIG. 18. Transverse momentum distributions of ϕ, K_0, Λ, $\bar{\Lambda}$ Ξ^-, $\bar{\Xi}^+$, Ω^-, $\bar{\Omega}^+$ in AuAu collisions at 11.5 GeV at central rapidity for different centralities. EPOS4 simulation (lines) are compared to data from STAR [29].

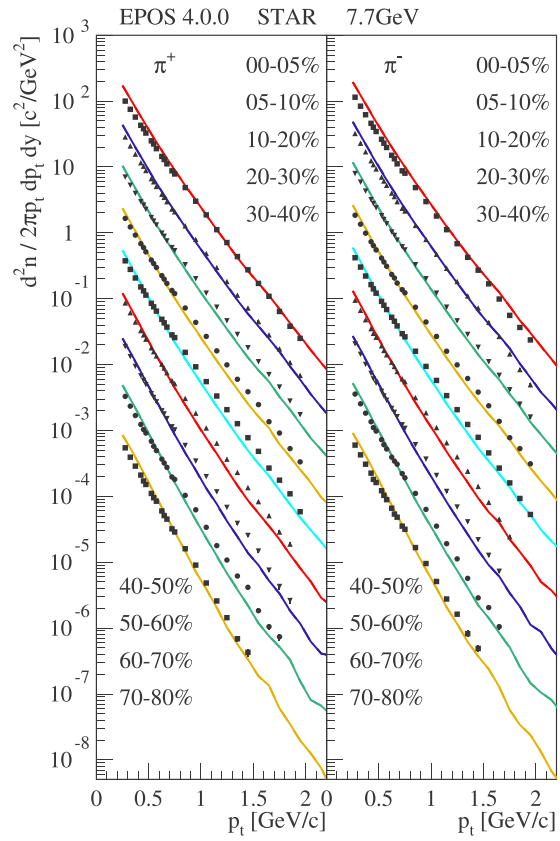

FIG. 19. Transverse momentum distributions of π^+, π^- in AuAu collisions at 7.7 GeV for different centrality classes. EPOS4 simulation (lines) are compared to data from STAR [28]. From top to bottom, we multiply the curves by 3^{-i}, $i = 0, 1, 2, 3, \ldots$.

are compared to data from STAR [28]. From top to bottom, we multiply the curves by 3^{-i}, $i = 0, 1, 2, 3, \ldots$.

In Fig. 18, we show transverse momentum distributions of ϕ, K_0, Λ, $\bar{\Lambda}$ Ξ^-, $\bar{\Xi}^+$, Ω^-, $\bar{\Omega}^+$ in AuAu collisions at 11.5 GeV at central rapidity for different centralities. EPOS4 simulation (lines) are compared to data from STAR [29].

Here we see for the first time (compared to higher energies) significant deviations between simulation and data. The most striking is a large proton excess at low p_t. And (as already seen earlier) a ϕ excess. Surprisingly, the hyperons are doing well.

E. Results for 7.7 GeV

In Figs. 19 and 20, we show transverse momentum distributions of π^+, π^-, K^+, K^-, p, $\bar{p}$ in AuAu collisions at 7.7 GeV for different centrality classes. EPOS4 simulation (lines) are compared to data from STAR [28]. From top to bottom, we multiply the curves by 3^{-i}, $i = 0, 1, 2, 3, \ldots$.

In Fig. 21, we show transverse momentum distributions of ϕ, K_0, Λ, $\bar{\Lambda}$ Ξ^-, $\bar{\Xi}^+$, Ω^-, $\bar{\Omega}^+$ in AuAu collisions at 19.6 GeV at central rapidity for different centralities. EPOS4 simulation (lines) are compared to data from STAR [29].

Here, at 7.7 GeV, essentially all spectra from the simulation are too soft, the yields at low p_t too high, with the biggest

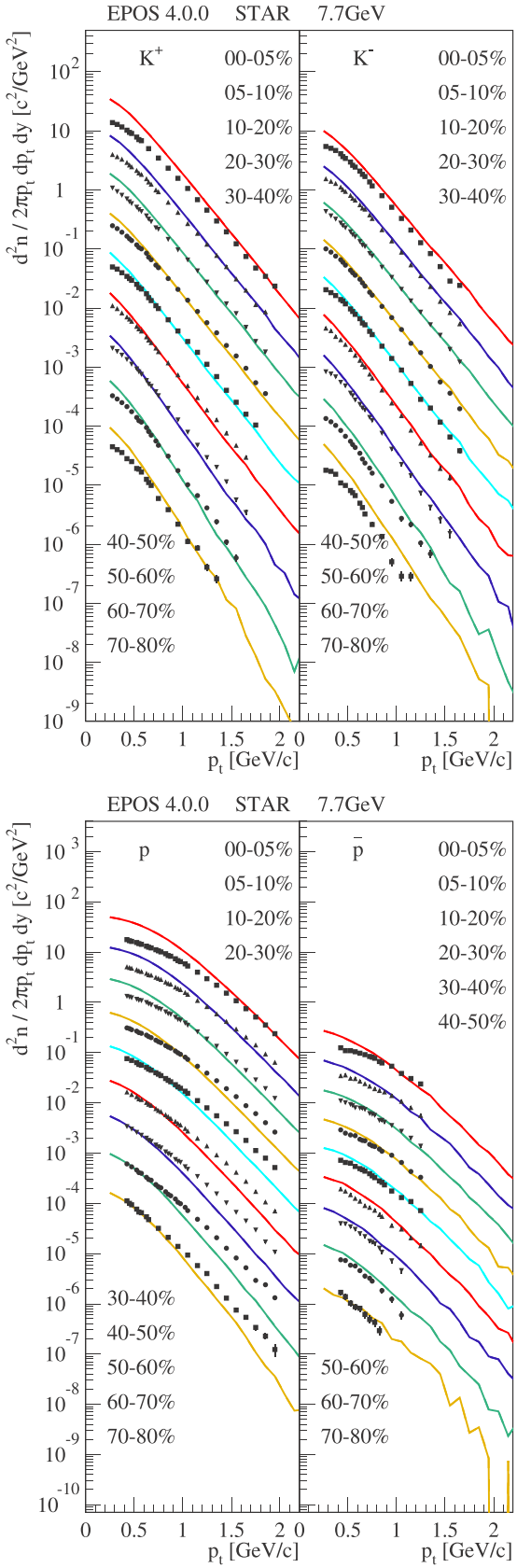

FIG. 20. Same as Fig. 19, but for K^+, K^-, p, $\bar{p}$.

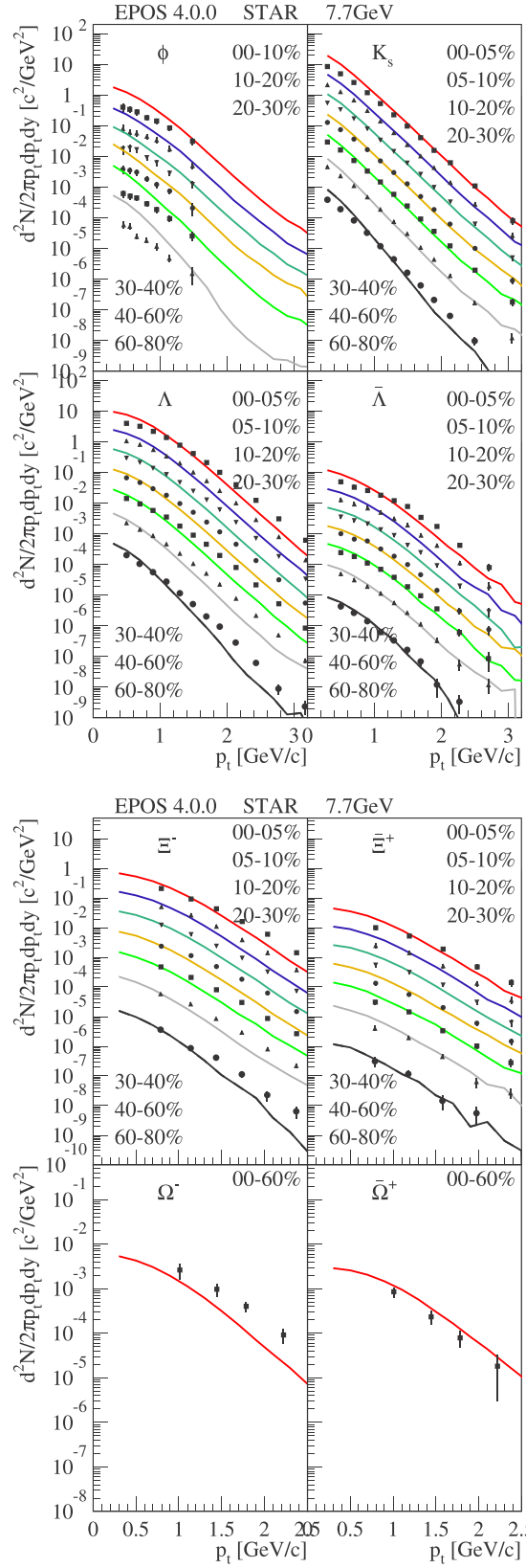

FIG. 21. Transverse momentum distributions of ϕ, K_0, Λ, $\bar{\Lambda}$ Ξ^-, $\bar{\Xi}^+$, Ω^-, $\bar{\Omega}^+$ in AuAu collisions at 19.6 GeV at central rapidity for different centralities. EPOS4 simulation (lines) are compared to data from STAR [29].

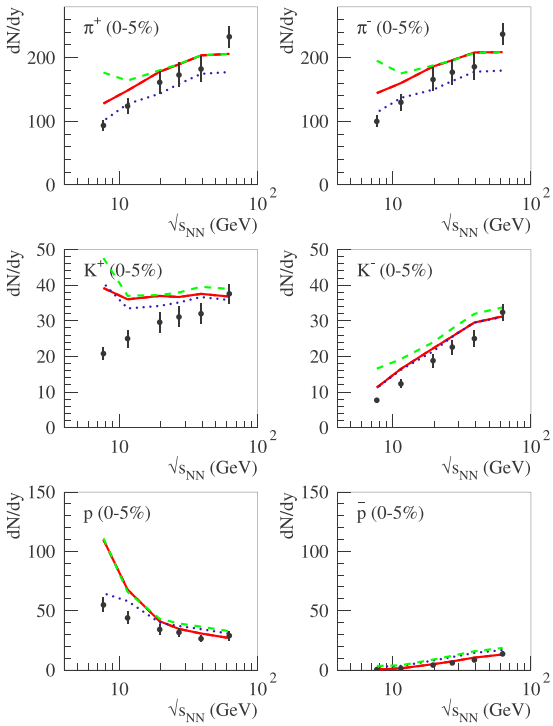

FIG. 22. Integrated yields of π^+, π^-, K^+, K^-, p, and $\overline{p}$ at midrapidity ($|y| < 0.1$) in the most central AuAu collision class (0–5%), as a function of collision energy $\sqrt{s_{NN}}$. EPOS4 simulation (lines) are compared to data from STAR [28].

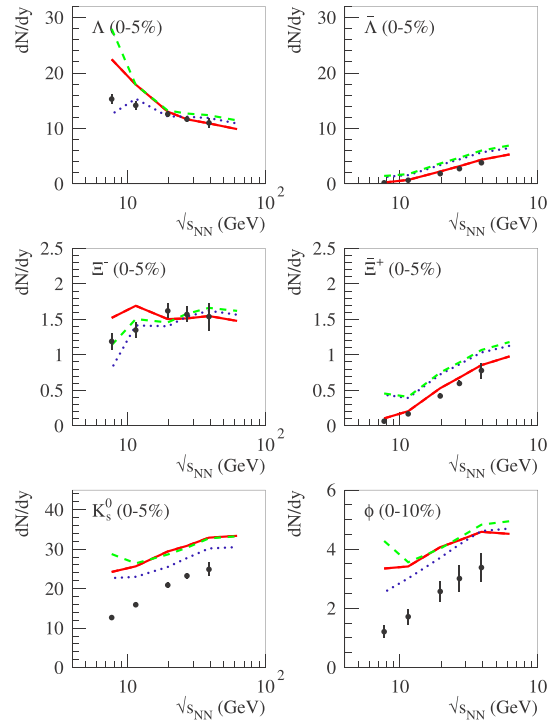

FIG. 23. Integrated yields of Λ, $\overline{\Lambda}$, Ξ^-, $\overline{\Xi}^+$, ϕ, K^0_s at midrapidity ($|y| < 0.5$) in the most central AuAu collision class (0–5%), as a function of collision energy $\sqrt{s_{NN}}$. EPOS4 simulation (lines) are compared to data from STAR [29].

excess observed for protons and K^+ mesons. So here the model does not work.

IV. RESULTS CONCERNING INTEGRATED YIELDS

In this section, we show the integrated yields dN/dy for every particle species as a function of $\sqrt{s_{NN}}$, at midrapidity in the most central AuAu collisions. We summarize thus the discussion from the previous section, by displaying how particle production changes with collision energy for every hadronic species, compared to STAR data from Refs. [28,29].

We compare in Fig. 22 the yields from EPOS4 (lines) of π^+, π^- K^+, K^-, p, and $\overline{p}$, measured within $|y| < 0.1$, with STAR data from Ref. [28]. We do the same in Fig. 23 for Λ, $\overline{\Lambda}$, Ξ^-, $\overline{\Xi}^+$, ϕ, and K^0_s, measured within $|y| < 0.5$, compared with STAR data from Ref. [29]. The red lines represent full EPOS4 simulations, blue dotted lines refer to core, green dashed lines refer to core + corona. For all hadronic species, the events considered are from the 0–5% centrality class, except for the ϕ mesons for which we consider 0–10% centrality events due to the available data. We only omit here Ω^- and $\overline{\Omega}^+$, as the data published by STAR in Ref. [29] is not using the same centrality classes for all energies, making it impossible to display meaningful results about the evolution of integrated yields with collision energy.

When looking at the whole ensemble of results, we see that particle production in EPOS4 simulations above 19.6 GeV is, overall, in good qualitative and quantitative agreement with STAR data. As expected, it reflects the conclusions from the last section. At lower energies, we observe a clear overproduction of protons, as well as Λ and Ξ^- baryons, unlike their respective anti-baryon counterparts. The yield of K^+ mesons is also largely overestimated at low energies. All this points to an overproduction of baryon number (in the form of too many u and d quarks), which is expected in the current construction of EPOS4 as "high-energy model," where all nucleon-nucleon interactions occur before particle production starts, which is clearly not correct at low energies.

Finally, the yield of K^0_s shown in Fig. 23 is overestimated for the whole range of collision energies displayed here, compatible with the p_t spectra at low p_t. However, its energy dependence follows qualitatively well the data.

V. RESULTS CONCERNING RAPIDITY DISTRIBUTIONS

Experimental (pseudo)rapidity distributions unfortunately do not exist for all RHIC BES energies (only for 62.4 and 19.6 GeV), but there are older results from the CERN Super Proton Synchrotron in this energy range, which we are going to show in addition, comparing EPOS4 simulations with data.

In Fig. 24, we show rapidity distributions for different centralities [from top to bottom: 0–3%, 6–10%, 15–20%, 25–35%, 35–40% (45–50%)] in AuAu collisions at 62.4 and 19.6 GeV. EPOS4 simulation (lines) are compared to data from PHOBOS (points) [30]. In Figs. 25 and 26, we show rapidity distributions for different centralities (from top to bottom: 0–5%, 5–10%, 10–15%, 15–20%, 20–25%, 25–35%)

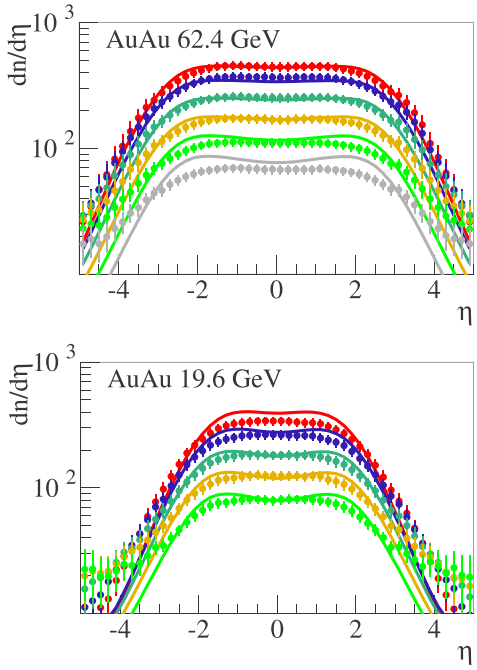

FIG. 24. Rapidity distributions for different centralities (see text) in AuAu collisions at 62.4 and 19.6 GeV. EPOS4 simulation (lines) are compared to data from PHOBOS (points) [30].

in fixed target (FT) PbPb collisions at 158 and 40 GeV. EPOS4 simulation (lines) are compared to data from NA50 (dots) [31]. For completeness, we should mention that the dotted lines in Figs. 25 and 26 refer to fits to the experimental data given in Ref. [31], the data itself are not published.

At 62.4, 19.6, and 158 GeV FT (≈17 GeV center-of-mass-system (CMS) energy) the simulated yields are reasonable compared to data, but there are more "plateaulike," i.e., too much remnant contributions. At very low energies (40 GeV FT, ≈9 GeV CMS energy) the simulated yields are too big, compatible with the results shown earlier.

Proton rapidity distributions are interesting, since they (more precisely: protons minus antiprotons) provide some information about the energy loss of the initial nucleons which constitute the two nuclei. In Fig. 27, we show rapidity distributions of protons (p) and antiprotons ($\bar{p}$) in central (0–10%)

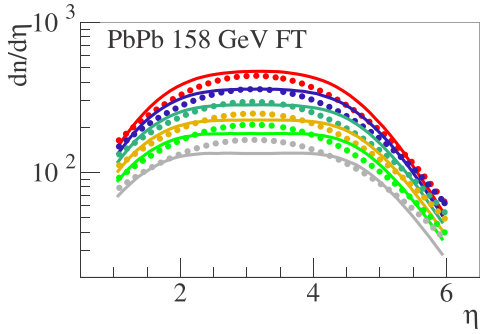

FIG. 25. Rapidity distributions for different centralities in fixed target (FT) PbPb collisions at 158 GeV. EPOS4 simulation (lines) are compared to data from NA50 (dots) [31].

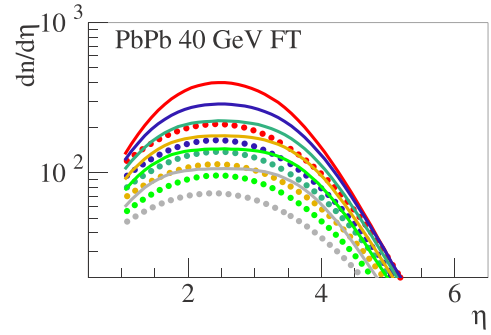

FIG. 26. Rapidity distributions for different centralities in fixed target (FT) PbPb collisions at 40 GeV. EPOS4 simulation (lines) are compared to data from NA50 (dots) [31].

AuAu collisions at 62.4 GeV. We show simulation results without (solid lines) or with (dashed lines) weak decay contributions. The reality is in between, since due to the detector geometry, not all weak decays actually happen before entering the detector. In Fig. 28, we show rapidity distributions of protons (p) and antiprotons ($\bar{p}$) for different centralities (from top to bottom: 0–5%, 5–12.5%, 12.5–23.5%, 23.5–33.5%, 33.5–43.5%) in FT PbPb collisions at 158 GeV (upper plot) and 40 GeV.

At 62.4 and 158 GeV FT (≈17 GeV CMS) the simulated yields are reasonable compared to data, but showing somewhat too much "stopping." At 40 GeV FT (≈9 GeV CMS energy), the simulated yields are too big, compatible with the results shown earlier.

VI. RESULTS CONCERNING V_2

In Figs. 29–34, the transverse momentum dependence of v_2 of identified particles within a pseudorapidity range of $|\eta| < 1$ in AuAu collisions at energies from 62.4 GeV down to 7.7 GeV are shown. Different centrality classes are considered: 0–10%, 10–40%, and 40–80%. We show full simulations (thick red lines) and those without hadronic cascade (thin green lines), and they are compared to data from STAR [34] in the Beam Energy Scan at the Relativistic Heavy Ion Collider. We employ the same event plane method as described in the experimental paper. For the upper plots, one should note that the

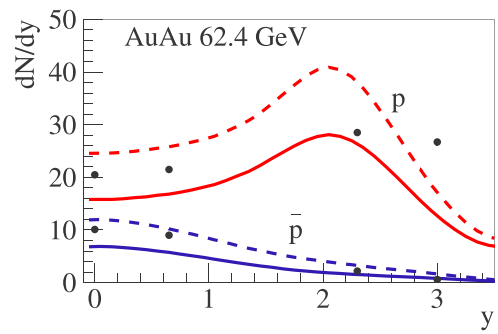

FIG. 27. Rapidity distributions of protons (p) and antiprotons ($\bar{p}$) in central (0–10%) AuAu collisions at 62.4 GeV. EPOS4 simulation (lines, see text) are compared to data from BRAHMS (points) [32].

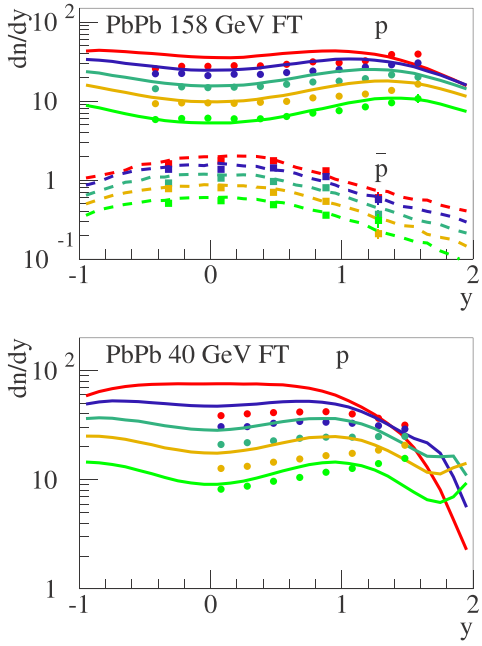

FIG. 28. Rapidity distributions of protons (p) and antiprotons ($\bar{p}$) for different centralities (see text) in fixed target (FT) PbPb collisions at 158 GeV (upper plot) and 40 GeV (lower plot). EPOS4 simulation (lines) are compared to data from NA49 (points) [33].

ranges on the ordinates change, depending on the centrality, since v_2 increases with decreasing centrality. In general, the simulation results describe the data reasonably well, also the centrality dependence. The biggest deviation is observed for protons for 40–80%. Also for the pions the agreement is not so great. But the hyperons (Ξ^- and Ω and their antiparticles $\bar{\Xi}^+$ and $\bar{\Omega}$) and as well the ϕ and the K_s are relatively close to the data.

VII. SUMMARY AND CONCLUSIONS

We reviewed briefly the EPOS4 approach, a detailed discussion can be found in Refs. [9–12]. Most important is the concept of parallel scattering of primary interactions, which is needed at high energies, to be more precise above 24 GeV [11]. We also reviewed briefly "secondary interactions" in EPOS4, composed of core-corona separation, hydrodynamic core evolution with subsequent decay (microcanonically), and final state hadron cascade

In the EPOS4 formalism, there is a smooth transition from high to low energy, certain features change (or disappear) gradually. The parton ladders become less frequent, they are replaced by soft Pomerons, and most importantly, the relative importance of particle production from remnant excitation and decay increases. We discussed how this affects the core-corona procedure. Below 30 GeV, even central rapidities are dominated by particle production from remnants, and essentially all prehadrons go into the core (for central collisions). We computed the energy densities of the core (the fluid initial condition) for the different systems, to observe that they drop from about 40 GeV/fm^3 at 5.02 ATeV to roughly 5 GeV/fm^3

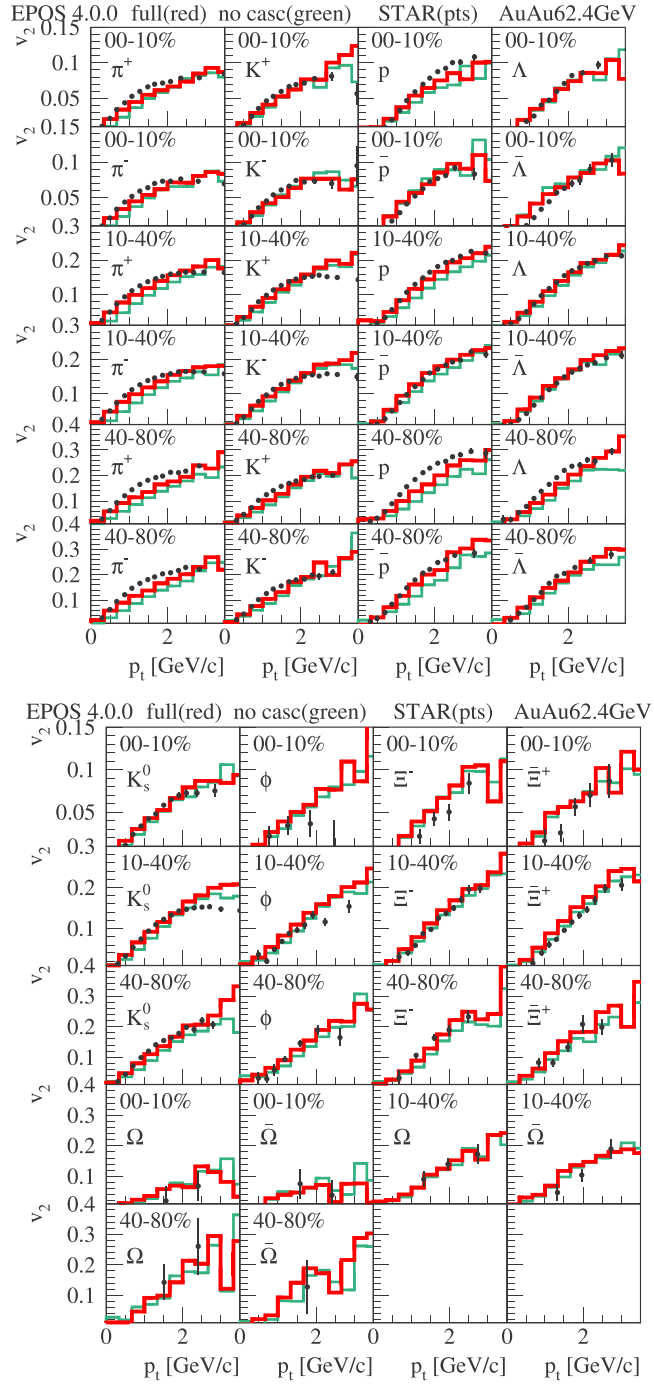

FIG. 29. Transverse momentum dependence of v_2 of identified particles in AuAu collisions at 62.4 GeV at central rapidity for different centralities. EPOS4 simulation, full simulations (thick red lines) and without hadronic cascade (thin green lines), are compared to data from STAR [34] (dots).

at 11.5 GeV, and then drop dramatically. At 4 GeV, there is no fluid anymore.

With all the model details already being published elsewhere [9–12], the main purpose of the paper is the presentation of a very detailed test, considering a very large set of experimental data in the RHIC energy domain, covering

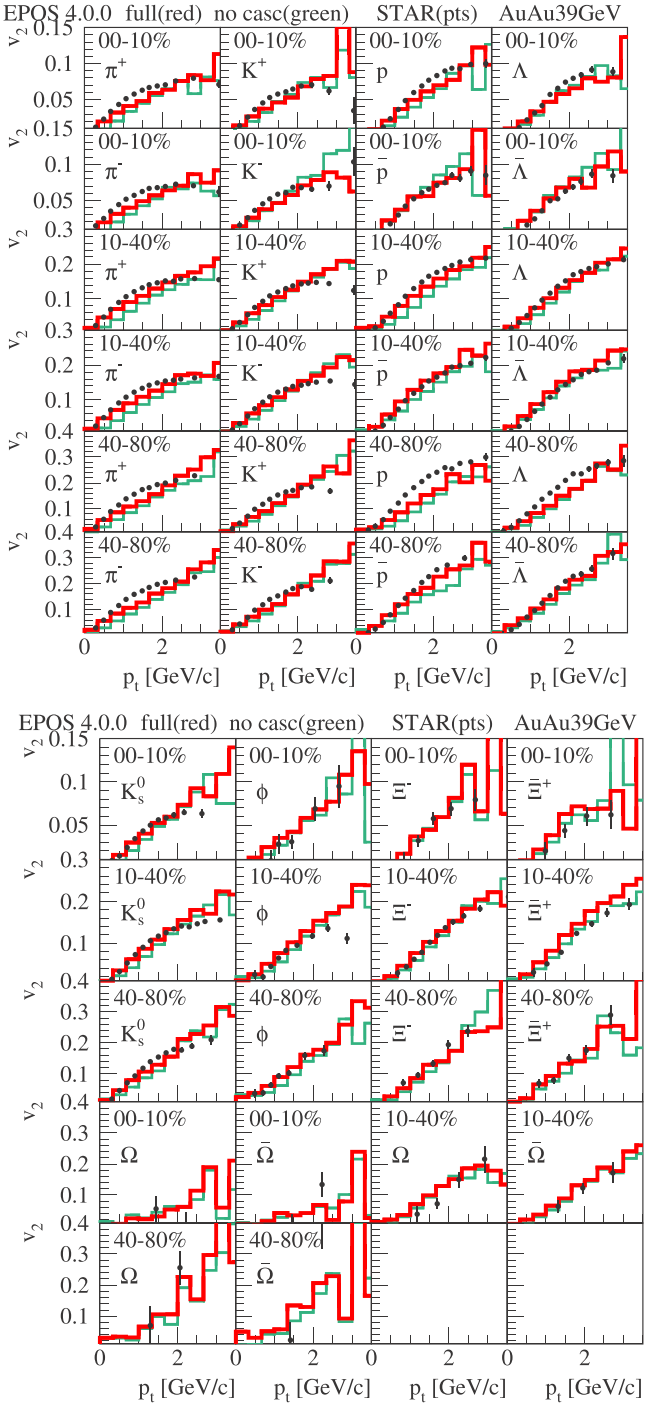

FIG. 30. Transverse momentum dependence of v_2 of identified particles in AuAu collisions at 39.4 GeV at central rapidity for different centralities. EPOS4 simulation, full simulations (thick red lines) and without hadronic cascade (thin green lines), are compared to data from STAR [34] (dots).

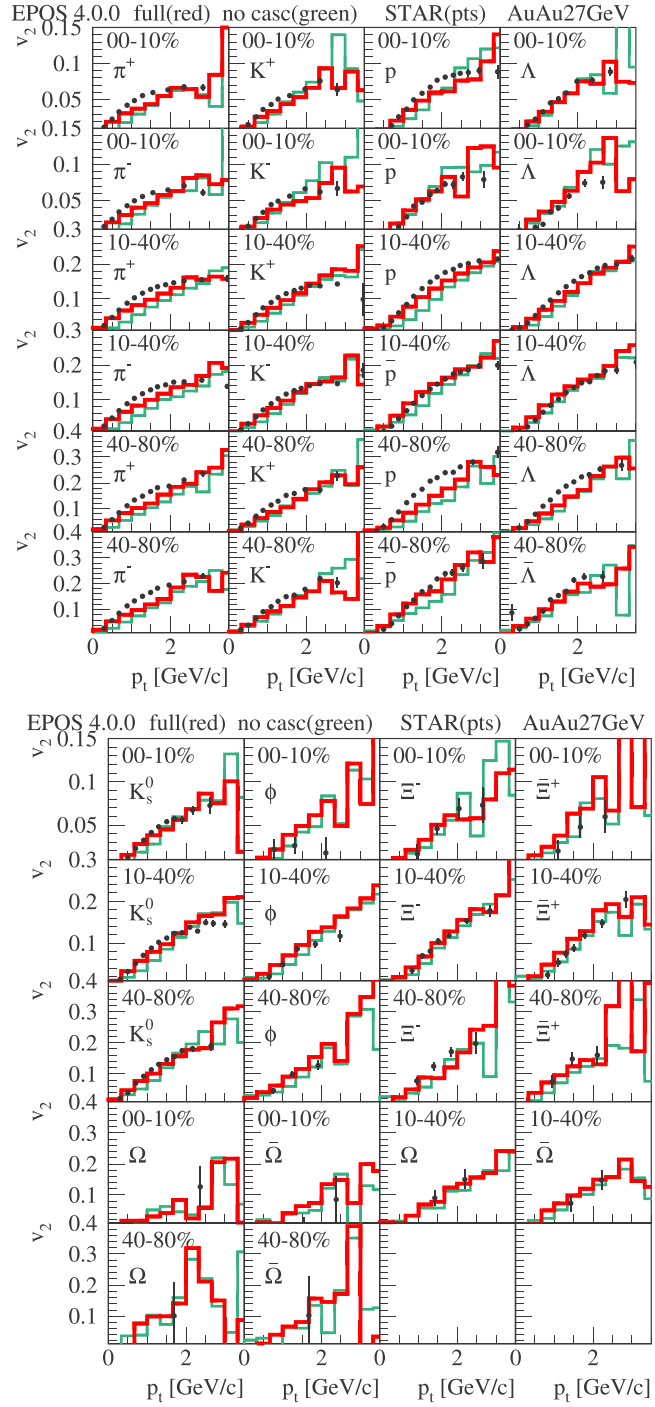

FIG. 31. Transverse momentum dependence of v_2 of identified particles in AuAu collisions at 27 GeV at central rapidity for different centralities. EPOS4 simulation, full simulations (thick red lines) and without hadronic cascade (thin green lines), are compared to data from STAR [34] (dots).

p_t spectra and also the p_t dependence of the elliptical flow, for identified particles. Spectra and v_2 provide complementary information about the fluid expansion. A particular aim was the investigation of a possible breakdown of the model at low energies, expected at around 24 GeV from theoretical considerations.

We first showed comparisons of simulations with data concerning p_t spectra of identified particles, from 39 GeV down to 7.7 GeV. For the higher energies, down to 19.6 GeV, the simulation results are relatively close to the data. At lower energies, we observe "problems." At 11.5 GeV, we see for the first time (compared to higher energies) significant deviations

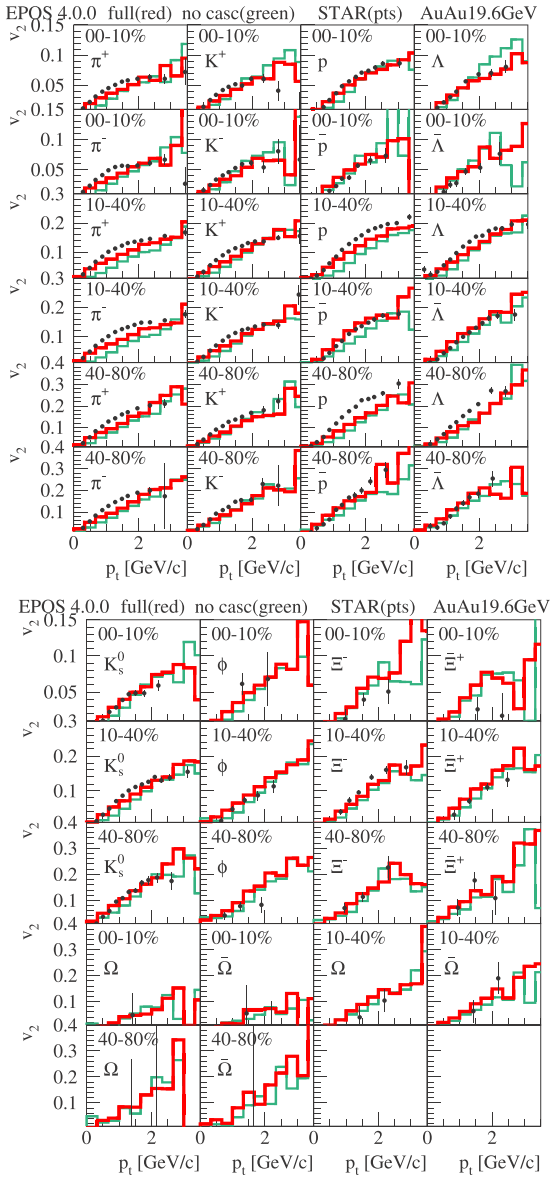

FIG. 32. Transverse momentum dependence of v_2 of identified particles in AuAu collisions at 19.6 GeV at central rapidity for different centralities. EPOS4 simulation, full simulations (thick red lines) and without hadronic cascade (thin green lines), are compared to data from STAR [34] (dots).

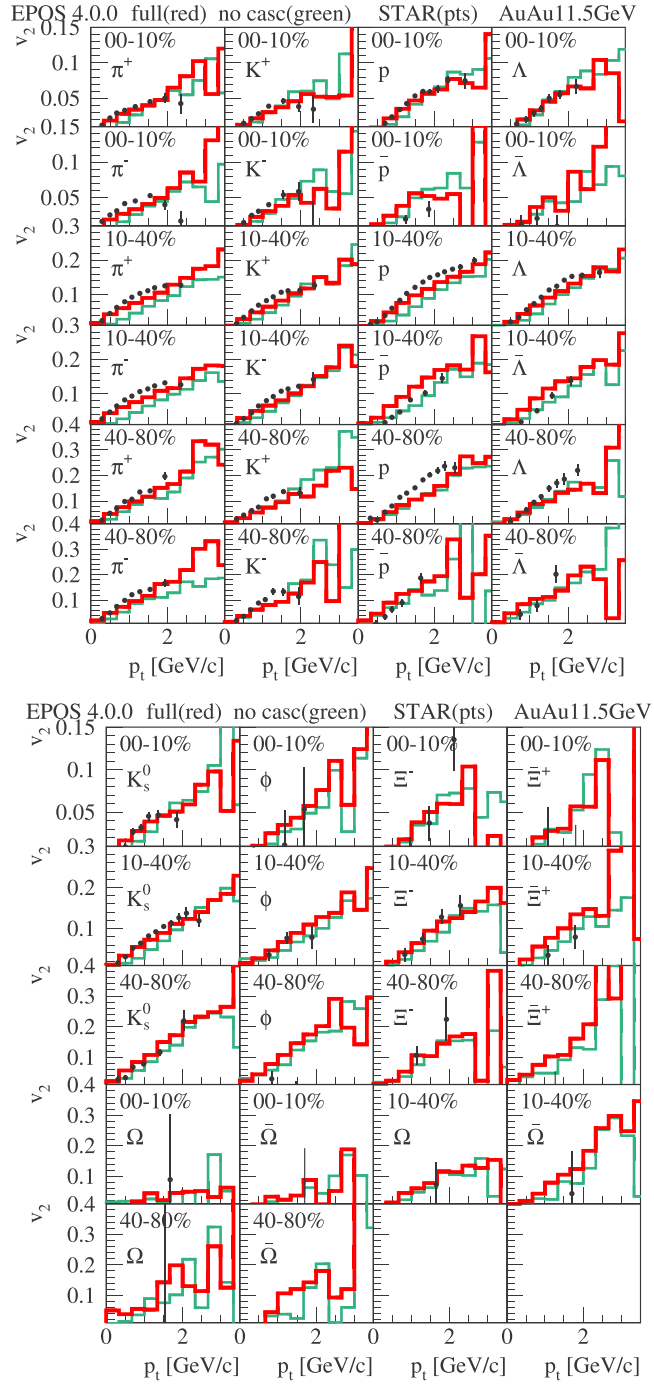

FIG. 33. Transverse momentum dependence of v_2 of identified particles in AuAu collisions at 11.5 GeV at central rapidity for different centralities. EPOS4 simulation, full simulations (thick red lines) and without hadronic cascade (thin green lines), are compared to data from STAR [34] (dots).

between simulation and data. The most striking is a large proton excess at low p_t. At 7.7 GeV, essentially all spectra from the simulation are too soft, the yields at low p_t too high, with the biggest excess observed for protons and K^+ mesons. So here the model does not work. These results concerning low p_t yields are also summarized, more globally, through the integrated yields of different hadronic species displayed as a function of energy in the most central collisions.

The situation is quite different concerning v_2. Here the simulation results describe the data reasonably well, also the centrality dependence. There is no "significant deterioration" at very low energies, as in the case of transverse momentum spectra. Although the model is obviously wrong at low energies, it works for v_2. But it is difficult to interpret these findings, since many thing are expected to change toward low energies, not only the scattering formalism (from parallel to sequential scatterings) but also, for example, the η/s values and the equation of state.

The success (at energies $\geqslant$19.6 GeV) and the failure (at energies below 19.6 GeV) of the model correspond

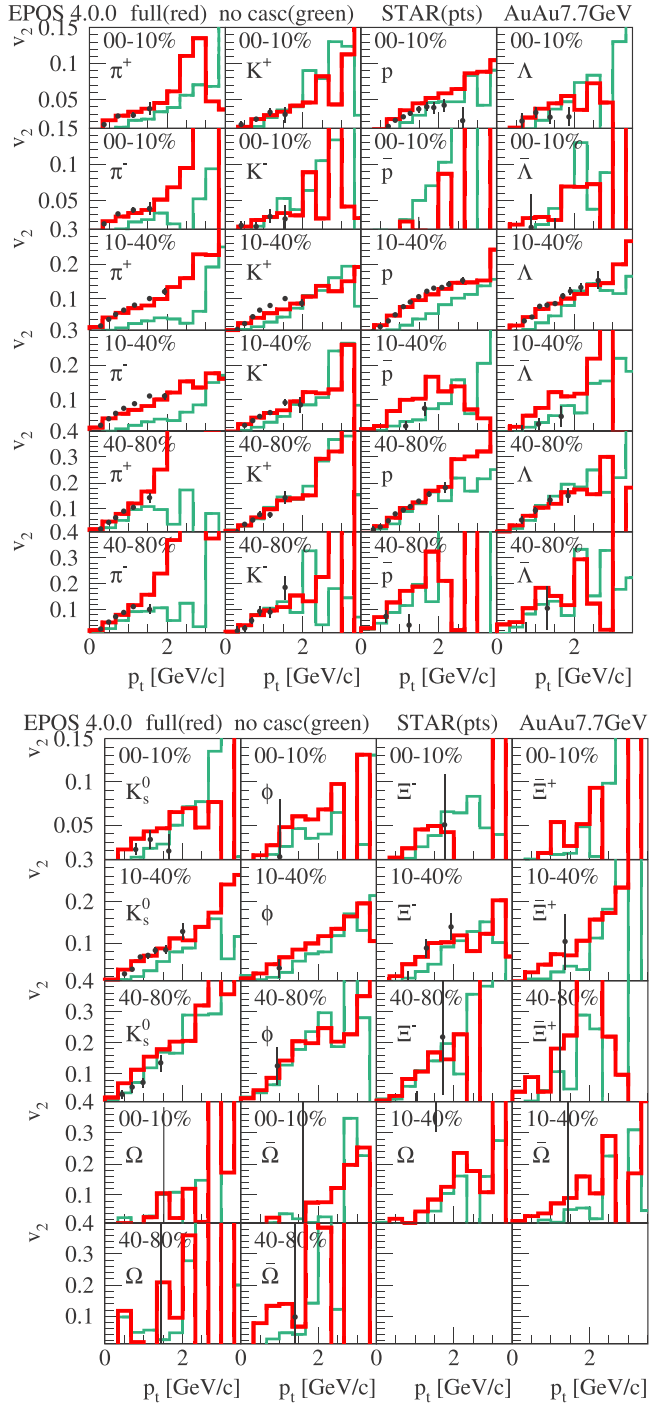

FIG. 34. Transverse momentum dependence of v_2 of identified particles in AuAu collisions at 7.7 GeV at central rapidity for different centralities. EPOS4 simulation, full simulations (thick red lines) and without hadronic cascade (thin green lines), are compared to data from STAR [34] (dots).

(amazingly well) to our earlier estimate of where the model should work and where not: it should work above 24 GeV (roughly estimated). The main problem of the (full) parallel scenario at low energies is the fact that a given nucleon hits all target nucleons on its way, although in reality it does not exist anymore for the final scatterings. This explains the large proton excess. One of the future projects will be to take that into account.

ACKNOWLEDGMENTS

I.K. acknowledges support by the Czech Science Foundation under No. 22-25026S. M.S. acknowledges support by U.S. Department of Energy Grant No. DE-SC0020651. J.J. acknowledges support by the MUSES collaboration under National Science Foundation (NSF) Grant No. OAC-2103680.

APPENDIX A: CORE AND CORONA CONTRIBUTIONS FOR 11.5 AND 7.7 GeV

In Figs. 35 and 36, we show ratios X/core+corona versus p_t, with X being the corona contribution (blue), the core (green), and the full contribution (red), for different hadrons. The four columns represent four different centrality classes, namely, 0–5%, 20–40%, 60–80%, and 80–100%. We show results for AuAu collisions at 11.5 and 7.7 GeV.

APPENDIX B: DECAY CHANNELS AND WEAK DECAY HANDLING

When counting particle yields, all excited states and their decays are considered. Particular care is needed for short lived resonances (with a lifetime of few fm/c). In that case, we consider the possibility that decay products rescatter in UrQMD, so we count all decays with decay products that do NOT

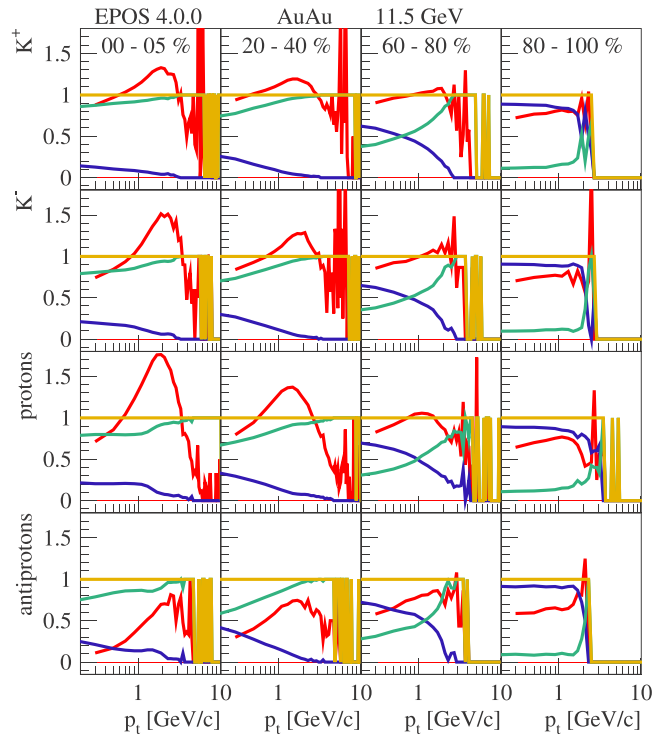

FIG. 35. The X/core + coron ratio, with X being the corona contribution (blue), the core (green), and the full contribution (red), for four centrality classes and four different particle species, for 11.5 GeV.

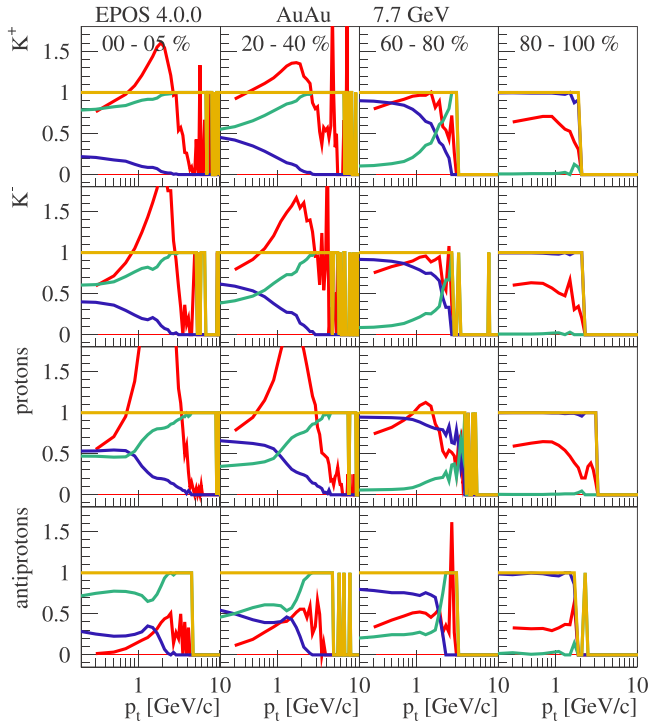

FIG. 36. Same as Fig. 35, but for 7.7 GeV.

rescatter, multiplied by 1/BR to compare with experiments which use the corresponding decay products to measure the resonance yield. In the present paper, this concerns the ϕ meson, where we consider $\phi \to K^+ + K^-$ and $\phi \to K^0 + \bar{K}^0$. For all other particles, we sum over all decay channels.

Concerning weak decays, they are done in EPOS4, but both parent and child particles are kept in the list. So in general, we may or not count weak decay products. Which option we choose, depends on the experimental setup (the detector geometry) and the question if they did (nor not) a feeddown correction.

Let us consider the STAR data from Ref. [28]. They say: "The (anti)protons also have a contribution of feed-down from weak decays of hyperons, which include particles which have not been measured. Contrary to pions, the analysis cut of DCA < 3 cm includes almost all daughter particles from hyperon decays." Based on this, in our case weak decay products are not counted, with the exception of protons and antiprotons. This statement is true for all results shown in Sec. III.

Although qualitative ("includes almost all"), we have some information concerning the STAR data from Ref. [28], which is not the case in other papers. So, for example, for the simulations compared to the BRAHMS data of Ref. [32], we show results for both cases (including or not weak decays). Here it seems that only a fraction of the particles decayed before entering the detector. For the other simulation results showing rapidity distributions of (anti)protons, decay products are not counted.

Concerning the v_2 results, weak decay products are not counted, and concerning the integrated yields, weak decay products are not counted, with the exception of (anti)protons and charged kaons.

[1] S. A. Bass *et al.*, Prog. Part. Nucl. Phys. **41**, 255 (1998).
[2] M. Bleicher *et al.*, J. Phys. G **25**, 1859 (1999).
[3] E. Bratkovskaya, W. Cassing, V. Konchakovski, and O. Linnyk, Nucl. Phys. A **856**, 162 (2011).
[4] W. Cassing and E. L. Bratkovskaya, Phys. Rev. C **78**, 034919 (2008).
[5] W. Cassing and E. Bratkovskaya, Nucl. Phys. A **831**, 215 (2009).
[6] P. Moreau, O. Soloveva, L. Oliva, T. Song, W. Cassing, and E. Bratkovskaya, Phys. Rev. C **100**, 014911 (2019).
[7] T. Song, H. Berrehrah, D. Cabrera, J. M. Torres-Rincon, L. Tolos, W. Cassing, and E. Bratkovskaya, Phys. Rev. C **92**, 014910 (2015).
[8] J. Weil *et al.*, Phys. Rev. C **94**, 054905 (2016).
[9] K. Werner, Phys. Rev. C **108**, 064903 (2023).
[10] K. Werner and B. Guiot, Phys. Rev. C **108**, 034904 (2023).
[11] K. Werner, Phys. Rev. C **109**, 034918 (2024).
[12] K. Werner, Phys. Rev. C **109**, 014910 (2024).
[13] V. N. Gribov, Zh. Eksp. Teor. Fiz. **53**, 654 (1967).
[14] V. N. Gribov, Sov. Phys. JETP **29**, 483 (1969).
[15] V. N. Gribov and L. N. Lipatov, Sov. J. Nucl. Phys. **15**, 438 (1972).
[16] V. A. Abramovskii, V. N. Gribov, and O. V. Kancheli, Yad. Fiz. **18**, 595 (1973).
[17] H. J. Drescher, M. Hladik, S. Ostapchenko, T. Pierog, and K. Werner, Phys. Rep. **350**, 93 (2001).
[18] G. Altarelli and G. Parisi, Nucl. Phys. B **126**, 298 (1977).
[19] Y. L. Dokshitzer, Sov. Phys. JETP **46**, 641 (1977).
[20] I. A. Karpenko, P. Huovinen, H. Petersen, and M. Bleicher, Phys. Rev. C **91**, 064901 (2015).
[21] C. Shen and B. Schenke, Phys. Rev. C **97**, 024907 (2018).
[22] C. Shen and B. Schenke, Phys. Rev. C **105**, 064905 (2022).
[23] C. Shen and S. Alzhrani, Phys. Rev. C **102**, 014909 (2020).
[24] K. Werner, Phys. Rev. Lett. **98**, 152301 (2007).
[25] K. Werner, B. Guiot, I. Karpenko, and T. Pierog, Phys. Rev. C **89**, 064903 (2014).
[26] I. Karpenko, P. Huovinen, and M. Bleicher, Comput. Phys. Commun. **185**, 3016 (2014).
[27] K. Werner, I. Karpenko, T. Pierog, M. Bleicher, and K. Mikhailov, Phys. Rev. C **83**, 044915 (2011).
[28] L. Adamczyk *et al.* (STAR collaboration), Phys. Rev. C **96**, 044904 (2017).
[29] J. Adam *et al.* (STAR collaboration), Phys. Rev. C **102**, 034909 (2020).
[30] B. Alver *et al.* (PHOBOS Collaboration), Phys. Rev. C **83**, 024913 (2011).
[31] M. C. Abreu *et al.* (NA50 Collaboration), Phys. Lett. B **530**, 43 (2002).
[32] I. C. Arsene *et al.* (BRAHMS Collaboration), Phys. Lett. B **677**, 267 (2009).
[33] T. Anticic *et al.* (NA49 Collaboration), Phys. Rev. C **83**, 014901 (2011).
[34] L. Adamczyk *et al.* (STAR Collaboration), Phys. Rev. C **93**, 014907 (2016).